Volume 3 | Issue 2 | August 2024
EISSN 2822-2318

Official Journal of Turkish Society of Magnetic Resonance

CRMRI

Current Research in MRI

AVES
curremr.com
TMRD
TÜRK MANYETİK REZONANS DERNEĞİ
TURKISH SOCIETY OF MAGNETIC RESONANCE

Current Research in MRI

TMRD
TÜRK MANYETİK REZONANS DERNEĞİ
TURKISH SOCIETY OF MAGNETIC RESONANCE

AVES

General Manager
Ali ŞAHİN

Journal Managers
Deniz KAYA
Irmak BERBEROĞLU

Publications Coordinators
Derya AZER
Nisanur ATICI
Şeref Mert GÜCÜN
Yiğit PEKZEREN
Lütfiye ÇETİN

Publications Technologies Coordinator
Ayça Nur SEZEN

Project Assistants
Batuhan KARA
Ozan ŞAHIN

Contact
Address: Büyükdere Cad. 199/6 34394 Mecidiyeköy, Şişli, İstanbul, Türkiye
Phone: +90 212 217 17 00
E-mail: info@avesyayincilik.com

Current Research in MRI

About the Current Research in MRI

Current Research in MRI is a peer reviewed, open access, online-only journal published by the Turkish Society of Magnetic Resonance.

Current Research in MRI is a triannual journal that is published in English in April, August, and December.

Indexing
Current Research in MRI is covered in the following indexing database;

- EBSCO

All content published in the journal is permanently archived in Portico.

Aims, Scope, and Audience
Current Research in MRI aims to publish studies of the highest scientific and clinical value. It also encourages the submission of high-quality research in the field of radiology.

Current Research in MRI covers a wide range of topics related to radiology.

Current Research in MRI publishes original articles, reviews, case reports, and letters to the editor that are prepared in accordance with ethical guidelines.

The target audience of the journal includes healthcare professionals, physicians, and researchers who are interested in or working in the field of radiology.

You can reach the current version of the instructions to authors at https://curremr.com/EN

Editor in Chief: Mecit Kantarcı
Address: Department of Radiology, Erzincan Binali Yıldırım University School of Medicine, Erzincan, Türkiye
E-mail: akkanrad@hotmail.com

Publisher: Turkish Society of Magnetic Resonance
Address: Konak Mah. 858. Sok. No: 2 Çakıroğlu İş Hanı Kat: 5 Daire: 55 Konak / İzmir, Türkiye

Publishing Services: AVES
Address: Büyükderece Cad., 199/6 34394 Şişli, İstanbul, Türkiye
Phone: +90 212 217 17 00
E-mail: info@avesyayincilik.com
Webpage: www.avesyayincilik.com

Current Research in MRI

CONTENTS

Current Research in MRI

Original Article

Trends in Gadolinium-Based Contrast Agents Use in Radiology Practice: A Retrospective Evaluation

Ozlem Celik Aydin[1], Huseyin Aydemir[2]

[1]Department of Pharmacology, Erzincan Binali Yıldırım University Faculty of Medicine, Erzincan, Türkiye
[2]Department of Radiology, Tokat Erbaa State Hospital, Tokat, Türkiye

Cite this article as: Aydin OC, Aydemir H. Trends in gadolinium-based contrast agents use in radiology practice: A retrospective evaluation. *Current Research in MRI*, 2024;3(2):35-38.

Corresponding author: Ozlem Celik Aydin, e-mail: ozlemclk_89@hotmail.com

Received: May 28, 2024 **Revision Requested:** June 10, 2024 **Last Revision Received:** June 12, 2024 **Accepted:** June 27, 2024
Publication Date: August 23, 2024

DOI:10.5152/CurrResMRI.2024.24098

Abstract

Objective: Contrast refers to the difference in signal strength in magnetic resonance imaging (MRI) that makes it possible to distinguish between different tissues. Contrast agents used in MRI can highlight the differences between tissues and organs, and reveal the differences between normal and pathological tissues. Gadolinium (Gd)-based contrast agents (GBCAs) are widely used in MRI to increase image contrast and enhance image quality.
Methods: GBCA usage data from January 1, 2020 to December 31, 2023 was obtained from hospital medical records. In terms of clinical characteristics, the total number of MRI examinations, the number of MRI examinations performed using GBCA, the number of MRI examinations performed without using GBCA, the type of GBCA used, the number of boxes prescribed, and the contrast volumes used were evaluated.
Results: A total of 167 295 MRI examinations were performed, with 9.8% (16 430/167 295) of these were taken using GBCA. The total number of patients who underwent contrast-enhanced MRI examination is 16 109. While the average age of the patients who underwent MRI examination was 52 years, it was determined that 57% of the patients were female and 43% were male. The number of GBCA boxes prescribed was 2394 in 2020, 3900 boxes in 2021, 4137 boxes in 2022, and 4956 boxes in 2023.
Conclusion: The use of GBCA in MRI increases the reliability and quality of diagnosis, and in our study, its use in our clinic is increasing over the years. To improve patient safety, we recommend that clinicians ensure that their use of GBCA is likely to add clinically meaningful information to imaging by making an individual risk benefit assessment for the patient. Our study will be useful for the radiologists to better understand new trends in contrast-enhanced MRI.
Keywords: MRI, gadolinium, contrast agents

INTRODUCTION

Magnetic resonance imaging (MRI) is a non-invasive and frequently used imaging method that creates diagnostic images using radiofrequency.[1] According to 2023 Organization for Economic Co-operation and Development (OECD) data, the number of MRIs performed per thousand people has the highest value among OECD countries in Türkiye.[2] In MRI, contrast refers to the difference in signal intensity that allows tissues to be separated from each other. Contrast agents applied using various methods (intravenous, oral, etc.) to increase this contrast can reveal the differences between normal and pathological tissues by highlighting the differences between tissues and organs.[3] Gadolinium-based contrast agents (GBCAs) are widely used in MRI to increase image contrast and improve image quality. The first GBCA, gadopentetate dimeglumine, was introduced for clinical use in 1988. The use of GBCAs has expanded the scope of application of MRI and allowed for more specific diagnoses. In the United States, GBCAs are used in 30%-45% of the approximately 40 million MRI examinations performed each year.[4] The use of these compounds is increasing day by day, and studies are continuing to develop new contrast agents.

Gd^{3+} is a heavy metal with 7 unpaired electrons and is highly toxic in its free ionic form, and can disrupt calcium-mediated signaling pathways. Therefore, in order to form a stable complex, it must be bound with a suitable ligand. All GBCAs consist of a Gd^{3+} with paramagnetic properties tightly bound to a chelating ligand. They are divided into macrocyclic/linear and ionic/nonionic agents according to ligand structure (Table 1).[4] Macrocyclic GBCAs have higher stability.[5] Most GBCAs are excreted renally. The choice of GBCA in clinical practice often depends on several variables, such as local protocols, physician expertise, patient expectations, financial constraints, molecule stability, and adverse effects.[6] Gadolinium-based contrast agents are administered intravenously. The approved standard dose of GBCA during a single imaging session is 0.1 mmol/kg.[7]

Gadolinium-based contrast agents are generally considered safe. However, following their application, mild adverse reactions such as nausea, vomiting, pain at the injection site, headache, and dizziness may occur. Additionally, disorders such as hypersensitivity reactions, nephrogenic systemic fibrosis, and gadolinium deposition disease have been reported. Gadolinium may accumulate in the brain and extracranial organs (bone, kidney,

Table 1. Gadolinium-Based Contrast Agents

Active Ingredient	Trade Name	Structure
Gadoterate meglumine (Gd-DOTA)	Dotarem (withdrawn from the Turkish market) Clariscan	Macrocyclic ionic
Gadobutrol (Gd-DO3A-butrol)	Gadovist	Macrocyclic nonionic
Gadodiamide (Gd-DTPA-BMA)	Omniscan (withdrawn from the Turkish market)	Linear nonionic
Gadopentetate dimeglumine (Gd-DTPA)	Magnevist Emaray	Linear ionic
Gadobenat dimeglumine (Gd-BOPTA)	MultiHance (withdrawn from the Turkish market)	Linear ionic
Gadoxetic acid disodium	Primovist	Linear ionic
Gadoversetamide (Gd-DTPA-BMEA)	Optimark	Linear nonionic

skin, and lymph nodes). The health effects of these accumulations have not yet been fully determined. More research and long-term follow-up are needed.[1,4] Regarding the prevention of gadolinium accumulation, especially in the brain, it has been recommended that GBCAs should be used only when medically necessary, the recommended dose should not be exceeded, and repeated applications should be avoided except for clinical indications.[8] In addition, in recent years, there have been suspicions that these substances may have genotoxic and cytotoxic effects, and studies on this subject are continuing.[9] It seems that their use should be approached with caution in clinical applications. During their use, it is necessary to evaluate the individual risk-benefit for the patient to ensure that there is a high probability of adding clinically meaningful information to the imaging.

Like all other biomedical products, the use of GBCA carries risks for patient health. There are studies in the literature evaluating the effectiveness, safety, and use of GBCAs. However, there are no studies reflecting real-life clinical data regarding the use of GBCAs in Türkiye. Our aim in this study is to determine the usage trends of GBCAs, which are frequently used in practice, in radiology clinics between 2020 and 2023. The findings we obtain from this study will guide the use of GBCAs.

MATERIAL AND METHODS

This study was approved by the Erzincan Mengücek Gazi Training and Research Hospital institutional ethics committee (Number: 2024-13/3, Session: 3, Date: 13.03.2024) and the ethics committee has waived the need for informed consent due to the methodology of the study.

Study Design

Our study was conducted retrospectively in the radiology clinic of a tertiary hospital. Gadolinium-based contrast agent usage data from January 1, 2020 to December 31, 2023 was obtained from hospital medical records.

Evaluated Variables

The research included patients from all age groups. Age and gender data were obtained for demographic characteristics. In terms of clinical characteristics, the total number of MRI examinations, the number of MRI examinations performed using GBCA, the number of MRI examinations performed without using GBCA, the type of GBCA used, the number of boxes prescribed, and the contrast volumes used were evaluated.

Statistical Analysis

Data were evaluated with the SPSS 20 program (IBM SPSS Corp.; Armonk, NY, USA). The Kolmogorov–Smirnov test was applied to determine whether the numerical values were normally distributed. Normally distributed data are presented as mean ± standard deviation. Categorical data are expressed as number (n) and percentage (%).

RESULTS

Magnetic resonance imaging examinations were performed on a total of 16 109 patients between January 1, 2020 and December 31, 2023. While the average age of the patients who underwent MRI examinations was 52, it was determined that 57% of the patients were female and 43% were male.

A total of 167 295 MRI examinations were performed between January 1, 2020 and December 31, 2023. Of these, 9.8% (16 430/167 295) were conducted using GBCA. The number and ratio of contrast-enhanced and non-contrast MRI examinations by year are presented in detail in Table 2. The number of contrast-enhanced examinations and patients by year is presented in detail in Table 3.

Of the 2394 boxes of GBCA prescribed in 2020, 7% were Gadodiamide (Omniscan), 37% were Gadoterate meglumine (Dotarem), and 56% were Gadobutrol (Gadovist). Of the 3900 boxes of GBCA prescribed in 2021, 25% were Gadoterate meglumine (Clariscan) and 75% were

Table 2. Number of MRI Examinations by Years

Year	Contrast-enhanced MRI Examination (%)	Non-contrast MRI Examination (%)	Total Examination (%)
2020	3545 (8.5)	38 223 (91.5)	41 768 (100)
2021	4479 (10)	40 275 (90)	44 754 (100)
2022	3842 (7.6)	46 448 (92.4)	50 290 (100)
2023	4564 (14.9)	25 919 (85.1)	30 483 (100)
Total	16 430 (9.8)	150 865 (90.2)	167 295 (100)

MRI, magnetic resonance imaging.

MAIN POINTS

- Gadolinium (Gd)-based contrast agents (GBCAs) are widely used in MRI to increase image contrast and improve image quality.
- A total of 167 295 MRI examinations were performed in our clinic between January 1, 2020 and December 31, 2023, and 9.8% (16 430/167 295) of them were performed using GBCA.
- The total number of patients who underwent contrast-enhanced MRI examinations was 16 109. While the average age of the patients who underwent MRI examinations was 52, it was determined that 57% of the patients were female and 43% were male.
- The use of GBCA in MRI increases the reliability and quality of diagnosis, and in our study, its use in our clinic has been increasing over the years. Our study will be useful for radiologists to better understand new trends in contrast-enhanced magnetic resonance.

Table 3. Number of Contrast Examinations and Number of Patients MRI Examination by Years

Year	Contrast-enhanced MRI Examination (n)	Patient (n)
2020	3545	3462
2021	4479	4398
2022	3842	3770
2023	4564	4479
Total	16.430	16.109

MRI, magnetic resonance imaging.

Gadobutrol (Gadovist). Of the 4137 boxes of GBCA prescribed in 2022, 25% were Gadoterate meglumine (Clariscan), 8% were Gadoterate meglumine (Dotarem), and 67% were Gadobutrol (Gadovist). In 2023, 20% of the total 4956 boxes of GBCA prescribed were Gadoterate meglumine (Clariscan) and 80% were Gadobutrol (Gadovist).

DISCUSSION

Macrocyclic ionic/nonionic and linear nonionic GBCAs were preferred in GBCA prescriptions. Guerbet Pharmaceuticals announced that Dotarem was withdrawn from the Turkish market on November 22, 2022. It has been observed that Dotarem had been preferred in MRI contrast agent prescriptions until that date.

The European Medicines Agency (EMA) suspended the license or restricted the use of some linear compounds, and later the US Food and Drug Administration announced that linear agents accumulate more in the brain than macrocyclic agents.[10,11] In 2017, the EMA allowed the use of the linear agents gadoxetic acid and gadobenate dimeglumine for limited indications (liver imaging), while suspending the use license of gadodiamide, gadopentate dimeglumine, and gadoversetamide. It has been reported that macrocyclic agents can continue to be used at the lowest dose that will provide optimal contrast and will not reduce diagnostic accuracy.[10,12]

In Europe, GBCAs are used properly for a variety of indications, demonstrating a significant improvement in diagnostic confidence. Following GBCA usage, it was established that GBCAs have a favorable safety profile, with findings for each agent employed being comparable (Clariscan, Dotarem (gadoteric acid), Gadovist (gadobutrol), and ProHance (gadoteridol)).[13]

In a European-based, multicenter, prospective study evaluating the use patterns of macrocyclic GBCAs in MRI of the central nervous system, gadoterate meglumine (Clariscan) was used in 66% (503) of cases, gadoterate meglumine (Dotarem) was used in 20% (160), gadobutrol (Gadovist) was used in 13% (97), and gadoteridol (ProHance) was used in 1% of the examinations.[6]

In a study evaluating the clinical use of the macrocyclic gadolinium-based contrast agent gadoterate meglumine (Clariscan) in 6 university hospitals in Korea, 1376 patients were included in the study during the evaluation period. The average volume of Clariscan used was 0.26 mL/kg. When MRI examinations were classified according to body regions, 69% included the nervous system, 13.6% the musculoskeletal system, and 4.9% the reproductive system. There were 14 adverse events in 10 patients, and Clariscan was generally well tolerated.[13]

In a prospective multicenter study in Europe, 2118 patients from 8 centers in 5 European countries were evaluated. Gadoterate meglumine (Clariscan) was used in 71.4% of the patients, gadoterate meglumine (Dotarem) in 16.8%, gadobutrol (Gadovist) in 11.2%, and gadoteridol (ProHance) in 0.6%. Most MRI examinations were performed for indications related to the central nervous system (46.2%). Adverse events were observed in 4 patients (0.19%).[14]

In conclusion, the use of GBCAs in MRI increases the reliability and quality of diagnosis, and in our study, its use in our clinic has been increasing over the years. In a non-comparative analysis with previous studies, no significant diagnostic difference was observed between GBCAs used in MRI in our clinic. To enhance patient safety, we advise clinicians to restrict the amount of GBCA administered, enhance patient education during GBCA administration, meticulously maintain institutional records of the volume and frequency of agents administered, and implement institutional outcome reviews and monitoring to detect gadolinium accumulation in patients receiving multiple doses. Our study will be useful for radiologists to better understand new trends in contrast-enhanced magnetic resonance.

Ethics Committee Approval: This study was approved by the Erzincan Mengücek Gazi Training and Research Hospital institutional ethics committee (Number: 2024-13/3, Session: 3, Date: 13.03.2024)

Informed Consent: N/A.

Peer-review: Externally peer-reviewed.

Author Contributions: Concept – H.A.; Design – H.A.; Supervision – H.A., O.C.A.; Resources – H.A., O.C.A.; Materials – O.C.A.; Data Collection and/or Processing – O.C.A.; Analysis and/or Interpretation – H.A., O.C.A.; Literature Search – O.C.A.; Writing Manuscript – H.A., O.C.A.; Critical Review – H.A., O.C.A

Declaration of Interests: The authors have no conflict of interest to declare.

Funding: The authors declared that this study has received no financial support.

REFERENCES

1. Iyad N, S Ahmad MS, Alkhatib SG, Hjouj M. Gadolinium contrast agents-challenges and opportunities of a multidisciplinary approach: literature review. *Eur J Rad Open*. 2023;11:100503. [CrossRef]
2. Yiğit V, Sağlık Teknolojisinin MRG. Yayılımı. *Turk Klin Sağlık Bilimleri Derg*. 2016;1(1):38-46.
3. Atman ED. *MRG'de Kontrast Artırma Yöntemleri ve MR Kontrast Maddeler*. 2020.
4. Cheong BY, Wilson JM, Preventza OA, Muthupillai R. Gadolinium-based contrast agents: updates and answers to typical questions regarding gadolinium use. *Tex Heart Inst J*. 2022;49(3):e217680. [CrossRef]
5. Çelik Aydin ÖÇ, AYDIN S, GÜNEY H. Kontrast ajanlar; Farmakolojik özellikleri, genel Advers Reaksiyonları ve İlaç Etkileşimleri. *Ank Eğitim Araştırma Hastanesi Tıp Derg*;53(1):61-67. [CrossRef]
6. Heshmatzadeh Behzadi AH, McDonald J. Gadolinium-based contrast agents for imaging of the central nervous system: A multicenter European prospective study. *Medicine*. 2022;101(34):e30163. [CrossRef]
7. Blomqvist L, Nordberg GF, Nurchi VM, Aaseth JO. Gadolinium in medical imaging—usefulness, toxic reactions and possible countermeasures—a review. *Biomolecules*. 2022;12(6):742. [CrossRef]
8. Costa AF, van der Pol CB, Maralani PJ, et al. Gadolinium deposition in the brain: a systematic review of existing guidelines and policy statement issued by the Canadian Association of Radiologists. *Can Assoc Radiol J*. 2018;69(4):373-382. [CrossRef]
9. Akbas E, Unal F, Yuzbasioglu D. Cellular toxicities of gadolinium-based contrast agents used in magnetic resonance imaging. *J Appl Toxicol*. 2023;43(7):958-972. [CrossRef]
10. Agency EM. *EMA's Final Opinion Confirms Restrictions on Use of Linear Gadolinium Agents in Body Scans*; 2017.

11. Food U, Drug Administration. *FDA Drug Safety Communication: FDA Approves Label Changes for Use of General Anesthetic and Sedation Drugs in Young Children*; 2017. FDA. Available at: https://www fda gov/drugs/drug-safety-and-availability/fda-drug-safety-communication-fda-approves-label-changes-use-general-anesthetic-and-sedation-drugs.
12. Agency EM. *Gadolinium-Containing Contrast Agents*. Amsterdam: European Medicines Agency; 2017.
13. Moon W-J, Cho YA, Hahn S, Son HM, Woo SK, Lee YH. The pattern of use, effectiveness, and safety of gadoteric acid (Clariscan) in patients undergoing contrast-enhanced magnetic resonance imaging: a prospective, multicenter, observational study. *Contrast Media Mol Imaging*. 2021;2021:4764348. [CrossRef]
14. Jakobsen JÅ, Quattrocchi CC, Müller FH, et al. Patterns of use, effectiveness and safety of gadolinium contrast agents: a European prospective cross-sectional multicentre observational study. *BMC Med Imaging*. 2021;21(1):74. [CrossRef]

Current Research in MRI

Original Article

Morphological Analysis of Temporomandibular Joint According to Gender and Age Groups

Merve Kolak[1], Volkan Kızılgöz[2]

[1]Erzincan Binali Yıldırım University, Oral and Dental Health Training and Research Hospital, Erzincan, Türkiye
[2]Department of Radiology, Erzincan Binali Yıldırım University Faculty of Medicine, Erzincan, Türkiye

Cite this article as: Kolak M, Kızılgöz V. Morphological analysis of temporomandibular joint according to gender and age groups. *Current Research in MRI*, 2024;3(2):39-42.

Corresponding author: Merve Kolak, e-mail: mervekolak@hotmail.com

Received: June 4, 2024 **Revision Requested:** June 15, 2024 **Last Revision Received:** July 8, 2024 **Accepted:** July 11, 2024
Publication Date: August 14, 2024

DOI:10.5152/CurrResMRI.2024.24100

Abstract

Objective: The purpose of this study was to assess the morphological parameters of the temporomandibular joint (TMJ) using magnetic resonance imaging in patients without TMJ pathologies. The findings of this investigation are expected to serve as reference values for clinical diagnosis and scientific research on temporomandibular disorders.

Methods: Magnetic resonance imaging images of 41 adult patients were examined. The condyle and glenoid fossa measurements were made in the sagittal plane. They were grouped by age, gender, and side, and statistical analysis was performed using the quantific anatomical values measured on magnetic resonance (MR) images.

Results: No statistical difference was observed between gender groups regarding all parameters. There was a significant, negative, low-level correlation between age and anterior condylar angle (ACoA) measurements on the left side. Considering the side comparisons, higher Glenoid Fossa Width (GFW) values ($P = .030$) were measured on the left side than on the right side. A significant, negative, low-level correlation between age and ACoA measurements was observed.

Conclusion: The correlation between age and ACoA measurements and GFW difference between different sides of the TMJ were the positive findings to be mentioned for his investigation. The morphological analyses focused on this anatomical region still need to be confirmed by the measurements performed on larger populations, since there are not many articles reporting specific results on this subject.

Keywords: Temporomandibular joint, anatomy, radiology, magnetic resonance imaging

INTRODUCTION

The temporomandibular joint (TMJ) is located between the fossa mandibularis and tuberculum articulare in the temporal bone and the caput mandibularis of the mandible. It is the only movable joint among the bones that make up the skull skeleton. There is an oval-shaped discus articularis between the joint surfaces. The discus articularis surrounds the joint surfaces all around and is adhered to the joint capsule. Temporomandibular joint is a synovial joint classified as a ginglymoarthrodial joint due to its surface shape and biaxial movements, rotational movement within the glenoid fossa, and translational movement along the articular process when opening the mouth.[1] Temporomandibular joint is one of the rarely encountered joints in the human body covered with fibrocartilage instead of hyaline cartilage.[2] It is thought that there is a certain correlation between the morphology of the TMJ and the functional loading from chewing forces.[3] The size and shape of the articular disc and condyle were found to be substantially correlated with the onset of TMD in earlier research. In particular, the articular disc's size and morphology tightly correlate with the disc's anterior displacement, and the condyle's size and morphology strongly correlate with the development of osteoarthritis.[4] There may be changes in TMJ morphology with aging, and differences between genders may occur.

Various imaging methods have been used to evaluate the morphology of the TMJ, such as panoramic radiography, computed tomography (CT), magnetic resonance imaging (MRI), cone beam computed tomography (CBCT), and ultrasound.[5-7] Magnetic resonance imaging is the most preferred imaging modality due to its high resolution of soft tissue and cartilage. Additionally, by using magnetic resonance, it has the advantage of being a non-ionizing radiation imaging procedure compared to CT.[8]

Temporomandibular disorders (TMDs) are the most common diseases in the mouth, teeth, and jaw area.[9] The aim of this study is to provide information to the literature by investigating the morphological properties of TMJ components with regard to age and gender groups using MR images.

MATERIAL AND METHODS

Patients

Our Institutional Ethics Committee approved this retrospective cross-sectional study. Since it was a retrospective study, informed consent was not required. This study has been approved by the Institutional Ethics Commitee of Clinical Researches Erzincan Binali Yıldırım University non-invasive clinical research ethics committee (Number: 348349 2024-04/02, Session: 03, Date: 21.03.2024).

After ethics committee approval, all patients in a certain period of time (August 1, 2020 to December 31, 2023) over the age of 18 who underwent MRI examination for TMJ were included in the study. In the image archives, patients with bone damage such as osteoarthritis, traumatic arthritis, and infectious arthritis, and patients whose MR images cannot be reached in the medical records and image archives were excluded. Patients whose MR images were not suitable for evaluation due to artifacts or technical deficiencies (n=2), and patients under the age of 18 (n=2) were not included in the study. Patients with non-contrast MRI examinations with indications such as muscle diseases, intra-articular deformities, disc dislocations, intra-articular inflammatory diseases, and mandibular hypomobilities were studied. Following exclusions, 41 patients were re-interpreted regarding the morphological properties of the TMJ.

Magnetic Resonance Imaging

All temporomandibular MR images were obtained using T2-weighted coronal, T2-weighted sagittal, and T1-weighted sagittal planes. Sagittal plane T1-weighted closed-mouth images were used for morphological assessments. The imaging parameters were as follows: field of view (FOV): 140 mm, time of repetition (TR): 643 ms, time of echo (TE): 17, slice thickness: 2.5 mm, voxel size: 0.5 × 0.5 × 2.5 mm for T1-weighted MR images.

Measurement Technique

We assessed the anterior–posterior length of condyles (AP LENGTHCo) in the sagittal plane MR images. AP LENGTHCo was measured as the interval between the most anterior and the posterior-most point of the condyle. The anterior condylar angle (ACoA) was assessed in the sagittal view as well and measured as the angle between the neck and head of the condyle using the anterior edges of these structures. Sagittal planes were also used for the articular fossa measurements. Glenoid Fossa Width (GFW) was determined as the distance between the post-glenoid process and the vertex of the joint eminence. The distance between the highest point of the fossa and the line between the post-glenoid process and the articular eminence vertex was considered for the assessment of the Glenoid Fossa Depth (GFD) in the study (Figure 1).

MAIN POINTS

- Previous studies revealed that the size and morphology of the mandibular condyle strongly related to temporomandibular dislocation onset.
- No significant statistical difference was found between male and female groups regarding the APLENGHTCo, GFW, GFD, ACoA measurements.
- A significant, negative, low level correlation between age and ACoA measurements was revealed on the left temporomandibular joint.
- Higher GFW values were measured for the left temporomandibular joint compared to the right side.

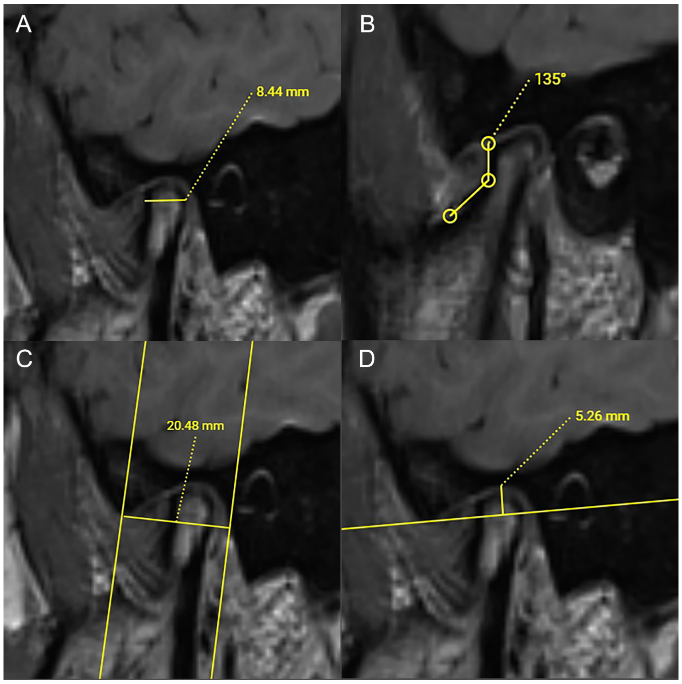

Figure 1. Measurement technique of the morphological parameters. The interval between the most anterior and posterior edges of the mandibular condyle as APLengthCo (A). ACoA was measured from the anterior edge, as the angle formed between the head and the neck of the mandibular condyle (B). GFW was determined as the distance between the post-glenoid process and the vertex of the joint eminence (C). The interval between the highest point of the fossa and the line between the post-glenoid process and the articular eminence vertex was considered as GFD (D). All measurements were performed on the sagittal MR images.

Statistical Analysis

Statistical analyses were performed using SPSS version 22.0 software program for Windows (IBM SPSS Corp.; Armonk, NY, USA). The percentage, frequency, mean, standard deviation, median, minimum, and maximum values were taken into account to be used or presented for descriptive statistics.

Glenoid fossa width, GFD, and APLENGHTCo values showed normal distribution in the Shapiro–Wilk Test. Therefore, parametric test procedures were used for comparisons regarding age and gender differences. In this context, the independent samples *t*-test was used to determine the relationship between the parameters. In order to perform the statistics regarding the ACoA, non-parametric tests were applied to indicate these relationships due to the data distribution characteristics. Thus, Mann–Whitney *U* and Spearman's rho correlation tests were carried out for this parameter and related statistical calculations.

The results were evaluated within the 95% CI, and a $P < .05$ was considered to indicate statistical significance.

RESULTS

There were 41 MRI images re-interpreted to reveal the morphological properties of the TMJ in this research (the mean age was 39.45 ± 14.02). Thirty-one (75.6%) of them were females, and 10 (24.4%) were males in the study group (Table 1).

No significant statistical difference was found between male and female groups regarding the APLENGHTCo, GFW, GFD, and ACoA

Table 1. The Measurement Results of the Morphological Parameters Regarding Sexes

	Female				Male				Total			
Parameter	**Min**	**Max**	**Mean**	**SD**	**Min**	**Max**	**Mean**	**SD**	**Min**	**Max**	**Mean**	**SD**
APLengthCo	2,73	10,27	6,03	1,60	3,50	7,83	5,35	1,33	2,73	10,27	5,86	1,56
ACoA	107,50	159,63	142,36	10,25	113,55	156,04	141,04	11,00	107,50	159,63	142,04	10,38
GFW	10,54	19,89	15,38	1,90	11,28	18,41	14,90	1,57	10,54	19,89	15,26	1,82
GFD	1,36	6,83	3,71	1,03	1,28	6,09	3,68	1,10	1,28	6,83	3,71	1,04

Min, Minimum value; Max, Maximum value; SD, Standart deviation; APLengthCo, Anteroposterior condyle length; ACoA, Anterior condyle angle; GFW, Glenoid fossa width; GFD, Glenoid fossa depth.

measurements. Age was another aspect studied in this research, and a significant, negative, low-level correlation between age and ACoA measurements on the left side.

In the comparison of the right and left sides for all of the measured parameters of the patients, a statistically significant difference for GFW value ($P=.030$) was observed, with higher GFW values measured on the left side compared to the right side for this parameter. APLENGHTCo, GFD, and ACoA values indicated no difference between the measurements on the left and the right sides.

DISCUSSION

This study focused on the versatility of the morphological features of the temporomandibular joint according to gender and age. According to the research results, no statistically significant differences were found when APLENGTHCo and GFD parameters were evaluated in terms of age, gender, and side. A significant, negative, low-level correlation was found between age and the left ACoA. When evaluated by side, it was seen that the GFW value of the left side was higher than on the right side.

The TMJ is one of the most significant and unique joints in the human body regarding its biomechanical features, but especially considering the cartilaginous content of this articulation. Understanding the anatomy of the TMJ is essential for distinguishing anatomical variations and pathological conditions.[10] Morphological variations of the components of the TMJ are significant in understanding the TMJ's normalcy, function, and potential pathological conditions, as well as offering suitable management and treatment.[11] Several studies have been undertaken to investigate the relationship between morphological and morphometric variations of the TMJ and their associations with pathological alterations based on gender and age.[12-14] The inclination of the articular eminence can affect the range of condyle excursion movement.[6] Patients with accentuated articular eminences had broader condyle–disc movement during function, which can increase the risk of elongating the posterior ligament and causing disc problems.[15] The articular eminence shape and inclination have also been identified as predisposing variables for disc dislocations.[15]

Even though the cortical borders of the bone can be visualized clearly by CT, MR images were chosen to perform the measurements in this study. The tendency of clinicians and surgeons to choose MRI instead of CT, due to the ability for detailed soft tissue imaging and visualization of the articular cartilage along with other bony compartments, provided a larger patient pool and data to study with a higher number of patients to measure.

In numerous reports mentioning temporomandibular dislocation, the morphological properties were revealed to be significantly associated with structural changes within the TMJ. Research shows that there is a relationship between condyle size and disc displacement. It is thought that the risk of developing TMD is higher in individuals with small condyle sizes.[16]

According to APLENGHTCo measurements, Coombs et al (n=22) and de Pontes (n=186) found that males had higher values than females in their study results, with both researchers using MR images to obtain data.[17,18] Regarding the studies using CBCT, Yasa et al (n=400) and Al-koshab et al (n=200) found higher APLENGHTCo measurement results in males parallel to those MRI studies.[19,20] In this current study, no significant statistical difference was found between males and females.

Derwich et al (n=210) performed GFD and GFW measurements using CBCT; however, the researchers did not evaluated the results in terms of gender. The average GFD was 9.8 mm and the average GFW was 20.5 mm according to their study results.[21] In this current research, GFD and GFW were evaluated and analyzed regarding age, gender, and different sides. The final results of this study indicated that only the left GFW values were higher than the right side, and no other differences were observed regarding these parameters in terms of age and gender.

There are few studies in the literature on ACoA measurements and the data distribution of this parameter concerning age and gender.

In the literature, ACoA measurements were mentioned in Torres et al's study; however, the study compared the patients with and without temporomandibular disc dislocations and did not address gender comparisons in normal individuals.[22] There was a significant, negative, low-level correlation on the left side between age and ACoA measurements in this current study presented to the literature.

Before analyzing the study results of this current research, readers should be aware of some limitations in planning, the study process, and considering the data pool of this investigation. First of all, the measurement data were examined based on a single reviewer's measurements, without considering intraobserver agreement. Having two or more reviewers would help compare results from different reviewers and identify interobserver differences. This would also be beneficial for the accuracy of the study results. The sample size of the study was relatively small, as the data were obtained from a single health center. A larger sample size, including different institutions or various geographical regions, would be better and may influence the study results. To maximize the study population, MR images were chosen as clinicians prefer this modality more than other imaging procedures to examine the joint and the articular disc simultaneously. However, CT images would be more effective to measure the bony morphology, which has been investigated in this research. The data obtained by radiological measurements on MR images could not be verified with a gold standard, such as surgical outcomes, and may not reflect accurate results as measurements performed in cadaveric studies. This situation can be considered another limitation of this study.

There is limited literature on the morphological analyses of the temporomandibular joint and its relationships with age and gender. This investigation found a significant, negative, low-level correlation between age and ACoA measurements. Additionally, both temporomandibular joints of each individual were compared with each other regarding the morphological parameters, and higher GFW values were measured on the left side compared to the right side for this anatomical approach.

Ethics Committee Approval: This study has been approved by the institutional ethics committee Ethics Commitee of Clinical Researches Erzincan Binali Yıldırım University non-invasive clinical research ethics committee (Number: 348349 2024-04/02, Session: 03, Date: 21.03.2024).

Informed Consent: N/A.

Peer-review: Externally peer-reviewed.

Author Contributions: Concept – M.K., V.K.; Design – M.K., V.K.; Supervision – V.K.; Resources – M.K., V.K.; Materials – M.K., V.K.; Data Collection and/or Processing – M.K., V.K.; Analysis and/or Interpretation – M.K.; Literature Search – M.K., V.K.; Writing Manuscript – M.K.; Critical Review – V.K.

Declaration of Interests: The authors have no conflict of interest to declare.

Funding: The authors declared that this study has received no financial support.

REFERENCES

1. Bag AK, Gaddikeri S, Singhal A, et al. Imaging of the temporomandibular joint: an up-date. *World J Radiol*. 2014;6(8):567-582. [CrossRef]
2. Vos LM, Kuijer R, Huddleston Slater JJR, Bulstra SK, Stegenga B. Inflammation is more distinct in temporomandibular joint osteoarthritis compared to the knee joint. *J Oral Maxillofac Surg*. 2014;72(1):35-40. [CrossRef]
3. Jiang H, Li C, Wang Z, et al. Assessment of osseous morphology of temporomandibular joint in asymptomatic participants with chewing-side preference. *J Oral Rehabil*. 2015;42(2):105-112. [CrossRef]
4. Bagis B, Ayaz EA, Turgut S, Durkan R, Özcan M. Gender difference in prevalence of signs and symptoms of temporomandibular joint disorders: a retrospective study on 243 consecutive patients. *Int J Med Sci*. 2012;9(7):539-544. [CrossRef]
5. Ahmed NF, Samir SM, Ashmawy MS, Farid MM. Cone beam computed tomographic assessment of mandibular condyle in Kennedy class I patients. *Oral Radiol*. 2020;36(4):356-364. [CrossRef]
6. Rabelo KA, Sousa Melo SL, Torres MGG, Campos PSF, Bento PM, Melo DP de. Condyle excursion angle, articular eminence inclination, and temporomandibular joint morphologic relations with disc displacement. *J Oral Maxillofac Surg*. 2017;75(5):938.e1-938.e10. [CrossRef]
7. Talmaceanu D, Lenghel LM, Bolog N, et al. Imaging modalities for temporomandibular joint disorders: an update. *Clujul Med*. 2018;91(3):280-287. [CrossRef]
8. Tomura N, Otani T, Narita K, et al. Visualization of anterior disc displacement in temporomandibular disorders on contrast-enhanced magnetic resonance imaging: comparison with T2-weighted, proton density-weighted, and precontrast T1-weighted imaging. *Oral Surg Oral Med Oral Pathol Oral Radiol Endod*. 2007;103(2):260-266. [CrossRef]
9. Wilentz JB, Cowley AW. How can precision medicine be applied to temporomandibular disorders and its comorbidities? *Mol Pain*. 2017;13:1744806917710094. [CrossRef]
10. Praveen BN SH. Morphological and radiological variations of mandibular condyles in health and diseases: A systematic review. *Dentistry*. 2013;03(1). [CrossRef]
11. Zhang Y, Xu X, Liu Z. Comparison of morphologic parameters of temporomandibular joint for asymptomatic subjects using the two-dimensional and three-dimensional measuring methods. *J Healthc Eng*. 2017;2017:5680708. [CrossRef]
12. Kurita H, Ohtsuka A, Kobayashi H, Kurashina K. Relationship between increased horizontal condylar angle and resorption of the posterosuperior region of the lateral pole of the mandibular condyle in temporomandibular joint internal derangement. *Dento Maxillo Facial Rad*. 2003;32(1):26-29. [CrossRef]
13. Sa SC, Melo SLS, Melo DP, Freitas DQ, Campos PSF. Relationship between articular eminence inclination and alterations of the mandibular condyle: a CBCT study. *Braz Oral Res*. 2017;31:e25. [CrossRef]
14. Margarida I, Crusoé-Rebello R, Sérgio P, et al. Evaluation of the relation between the horizontal condylar angle and the internal derangement of the TMJ-a magnetic resonance imaging study Avaliação da relação entre o ângulo horizontal do côndilo e o desarranjo interno da ATM, por meio de ressonância magnética. *Pesqui Odontol Bras*. 2003;17(2):176-182.
15. Sharma S, Gupta DS, Pal US, Jurel SK. Etiological factors of temporomandibular joint disorders. *Natl J Maxillofac Surg*. 2011;2(2):116-119. [CrossRef]
16. Guercio Monaco E, De Stefano AA, Hernandez-Andara A, Galluccio G. Correlation between condylar size on CT and position of the articular disc on MRI of the temporomandibular joint. *Cranio*. 2022;40(1):64-71. [CrossRef]
17. de Pontes MLC, Melo SLS, Bento PM, Campos PSF, de Melo DP. Correlation between temporomandibular joint morphometric measurements and gender, disk position, and condylar position. *Oral Surg Oral Med Oral Pathol Oral Radiol*. 2019;128(5):538-542. [CrossRef]
18. Coombs MC, Bonthius DJ, Nie X, Lecholop MK, Steed MB, Yao H. Effect of measurement technique on TMJ mandibular condyle and articular disc morphometry: CBCT, MRI, and physical measurements. *J Oral Maxillofac Surg*. 2019;77(1):42-53. [CrossRef]
19. Al-Koshab M, Nambiar P, John J. Assessment of condyle and glenoid fossa morphology using CBCT in South-East Asians. *PLoS One*. 2015;10(3):e0121682. [CrossRef]
20. Yasa Y, Akgül HM. Comparative cone-beam computed tomography evaluation of the osseous morphology of the temporomandibular joint in temporomandibular dysfunction patients and asymptomatic individuals. *Oral Radiol*. 2018;34(1):31-39. [CrossRef]
21. Derwich M, Mitus-Kenig M, Pawlowska E. Temporomandibular joints' morphology and osteoarthritic changes in cone-beam computed tomography images in patients with and without reciprocal clicking-A case control study. *Int J Environ Res Public Health*. 2020;17(10). [CrossRef]
22. Torres MGG, Crusoé-Rebello IM, Rosário M, Albuquerque MC, Campos PSF. Morphometric features of the mandibular condyle and association with disk abnormalities. *Oral Surg Oral Med Oral Pathol Oral Radiol*. 2016;121(5):566-572. [CrossRef]

Current Research in MRI

Original Article

Evaluating Efficacy of Dynamic MR Perfusion Imaging in Soft Tissue Tumors

Idris Ozdas[1], Muhammet Firat Oztepe[1], Nil Tokgoz[2], Murat Ucar[2]

[1]Department of Radiology, Batman Training and Research Hospital, Batman, Türkiye
[2]Department of Radiology, Gazi University Faculty of Medicine, Ankara, Türkiye

Cite this article as: Ozdas I, Firat Oztepe M, Tokgoz N, Ucar M. Evaluatıng efficacy of dynamic MR perfusion imaging in soft tissue tumors. *Current Research in MRI*, 2024;3(2):43-48.

Corresponding author: Idris Ozdas, e-mail: idrisozdas@gmail.com

Received: June 7, 2024 **Revision Requested:** July 9, 2024 **Last Revision Received:** July 9, 2024 **Accepted:** July 15, 2024
Publication Date: August 21, 2024

DOI:10.5152/CurrResMRI.2024.24101

Abstract

Objective: The aim of this study was to assess the effectiveness of dynamic contrast-enhanced (DCE) MRI perfusion parameters and signal intensity–time curves in distinguishing between benign and malignant soft tissue tumors.
Methods: The study included 51 patients with soft tissue tumors who underwent DCE MRI at 3.0 T. Among these patients, 30 had benign tumors, while 21 had malignant tumors. Perfusion parameters such as k-trans, kep, Ve, and iAUC were measured. Calculations were performed at the most contrast-enhanced areas of the lesions using circular regions of interest measuring 0.2-0.4 cm². The findings were illustrated using signal intensity–time (SIT) curves, which were categorized into 5 types for evaluation.
Results: In the benign group, 19 out of 30 lesions (63.3%) showed contrast enhancement patterns corresponding to type 1-2 SIT curves, and 11 out of 30 lesions (36.7%) exhibited patterns corresponding to type 3-4-5 SIT curves. In contrast, all 21 malignant lesions (100%) displayed type 3-4-5 patterns. Mean values of K-trans ($P < .001$), Ve ($P = .004$), and iAUC ($P < .001$) were significantly higher in malignant lesions compared to benign ones. There was no significant difference in Kep values between the 2 groups ($P = .628$).
Conclusion: The perfusion parameters K-trans, Ve, and iAUC, along with the contrast enhancement patterns observed in DCE MRI, can aid in differentiating between benign and malignant soft tissue tumors.
Keywords: Dynamic contrast-enhanced MRI, soft tissue tumors, MRI perfusion

INTRODUCTION

Magnetic resonance imaging (MRI) is a widely used imaging method in the investigation of soft tissue tumors due to its superiority in soft tissue contrast.[1,2] Morphological features of tumors, such as size, extension, and relationship with vascular structures can be evaluated with conventional MRI sequences. Administration of paramagnetic contrast material can support the evaluation of these features.[1-6] These agents pass from the intravascular space to the extravascular space, thus enabling both the detection and characterization of tumors by MRI.[7]

Contrast-enhanced MRI can be applied statically and dynamically. In static contrast MRI, a tissue signal is obtained at a random time point following the injection of contrast material. In contrast to static contrast-enhanced MRI, dynamic contrast-enhanced (DCE) MRI samples the MR signal at multiple time points following the injection of contrast medium. This gives information about the area's enhancement over time. These enhancement characteristics show tissue vascularity and perfusion, which may be associated with tumor angiogenesis.[1,8]

Differentiating benign and malignant soft tissue tumors is important for patient management and treatment planning. Making this distinction prevents unnecessary surgery in benign lesions. With developing MRI technology, it is becoming a candidate for a non-invasive method in the differential diagnosis of benign and malignant soft tissue tumors. There are some publications showing that perfusion MRI parameters can be used to differentiate benign and malignant tumors.[9-12]

The aim of this study was to assess the effectiveness of DCE-MRI perfusion parameters and signal intensity–time curves in differentiating benign and malignant soft tissue tumors.

MATERIAL AND METHODS

Patient Selection

This retrospective study received approval from Gazi University ethics committee with decision number: 513, and informed consent was waived. Sixty-four patients who underwent DCE-MRI between January 2011 and November 2014 with the diagnosis of soft tissue tumors were evaluated.

Patient data were collected from the hospital medical recording and data system. Patients with soft tissue tumors that were histopathologically confirmed or diagnosed through clinical and radiological follow-ups were included in this study. Patients whose DCE-MRI was not performed with the appropriate technique and whose images not suitable for evaluation were excluded from the study.

MRI Technique

All cases were examined by a 3.0 T MR system (Magnetom Verio, Siemens, Erlangen, Germany), with body coils or superficial coils depending on the localization of the lesion. Before the administration of the contrast agent, the standard T1W and T2W SE sequence images were acquired, and then DCE-MRI was performed.

For the DCE-MRI, all cases were administered gadopentetate dimeglumine (Magnevist, Bayer-Schering, Berlin, Germany) 0.1 mmol/kg intravenously. Following the administration of the intravenous contrast agent, 15 mL of physiological saline solution was given at the same rate. Dynamic contrast-enhanced-MRI sequencing started simultaneously with the administration of the IV contrast media injection. Dynamic contrast-enhanced-MRI was performed using 3-dimensional fat-suppressed T1W GRE (VIBE – Volumetric Interpolated Breath-hold Examination) sequences. The following parameters were used for the T1W VIBE sequences: TR: 4.29, TE: 1.47, NEX: 1, flip angle: 9°, FOV: 280 mm, matrix: 183 × 288, and slice thickness: 4 mm. Images were acquired in 35 consecutive sequences, each lasting 10-15 seconds and covering all lesions on the axial plane.

The computations were performed at the highest contrast-enhanced areas of the lesions using circular region of interests (ROIs) of 0.2-0.4 cm^2. The results were demonstrated by the signal intensity–time (SIT) curves. Signal intensity–time curves were evaluated in 5 categories.[11]

Type 1: No contrast enhancement.
Type 2: Slow contrast enhancement.
Type 3: Plato phase following the rapid enhancement at the beginning.
Type 4: Wash-out phase following the rapid enhancement at the beginning.
Type 5: Increasingly contrast enhancement following the initial rapid enhancement.

The following DCE-MRI perfusion parameters were *K-trans* (volume transfer constant), *kep* (transfer rate constant, which is the reflux of contrast agent from the extravascular extracellular space to the plasma compartment), *Ve* (fractional volume of the extravascular extracellular space), and *iAUC* (the initial area under the contrast uptake curve) values computed at the highest contrast-enhanced areas of the lesions using circular ROI of 0.2-0.4 cm^2. Simultaneously, circular ROI were placed in the arteries and muscles to compute the perfusion parameters.

Statistical Analysis

The statistical tests were performed in SPSSversion 20(IBM SPSS Corp.; Armonk, NY, USA). Primarily, descriptive analyses were utilized. The Shapiro–Wilk normality test was used to determine whether the data followed a normal distribution. For continuous variables, descriptive statistics were presented as mean ± SD or as median values (minimum–maximum). Categorical variables were expressed as numbers of observations and percentages (%). The Mann–Whitney *U* test was used to evaluate the differences between the benign and malignant lesion groups. The cut-off points for the parameters were determined by receiver operating characteristic (ROC) analysis to assess the values of the T1W dynamic perfusion MRI parameters useful for the differential diagnosis of benign and malignant lesions. Using these cut-off points of the parameters, the values for sensitivity and specificity, as well as the positive predictive values (PPV) and negative predictive values (NPV) were determined according to Youden's index. To evaluate whether the k-trans, kep, Ve, and iAUC values were determinants for the differential diagnosis of malignant and benign lesions, the areas under the curve were calculated by ROC analysis. If the value of the area under the curve was found to be significant, the best cut-off point was calculated using Youden's index. In addition, the sensitivity, specificity, and reliability values, as well as the positive and negative predictive values were calculated for this point. $P < .05$ was considered statistically significant.

RESULTS

A total of 51 cases were included in the study, comprising 24 (47.1%) female and 27 (52.9%) male patients. The patients' ages ranged 12-84 years, with a mean age of 42.2 ± 19.5. Of the cases, 30 (58.8%) were diagnosed with benign soft tissue tumors, 16 (31.4%) with malignant tumors, and 5 (9.8%) were diagnosed with intermediate–borderline soft tissue tumors. The diagnoses were made histopathologically in 34 patients and through clinical and radiological follow-up findings in 17 patients. Intermediate-borderline tumors were included in the malignant tumors group. Finally, 30 (58.8%) cases with benign soft tissue lesions and 21 (41.2%) malignant tumor cases, making up a total of 51 cases, were included in our study. Histopathological subtypes of tumors are presented in Table 1.

No statistically significant differences were found in age, gender, and the mean dimension of the lesions between the malignant and benign soft tissue lesion groups ($P > .05$). The comparisons of the benign and malignant cases in terms of age, gender, and the mean dimension of the lesions are presented in Table 2.

The distribution of the SIT curve categories is detailed in Table 3. Nineteen (63.3%) lesions demonstrated contrast enhancement patterns of types 1 and 2; however, 11 (36.7%) cases demonstrated type 3, 4, and 5 SIT curve categories out of the 30 benign lesions. On the other hand, all 21 (100%) malignant soft tissue tumors showed type 3, 4, and 5 contrast agent enhancement patterns. Therefore, the NPVs of type 1 and 2 SIT curve patterns were found to be 100% in diagnosing malignant lesions.

The distributions of the perfusion parameters, computed from T1W dynamic perfusion MRI, in benign and malignant lesion groups are presented in Table 4.

MAIN POINTS

- This study evaluates the effectiveness of dynamic contrast-enhanced (DCE) MRI perfusion parameters and signal intensity–time (SIT) curves in differentiating benign and malignant soft tissue tumors.
- Significant differences in K-trans, Ve, and iAUC values were found between benign and malignant tumors, with higher values observed in malignant tumors, aiding in their differentiation.
- DCE MRI provides useful quantitative parameters and SIT curves for distinguishing between benign and malignant soft tissue lesions.

Table 1. Histopathological Subtypes of Tumors

Histopathological Subtypes	n
Benign (n=30)	
Lipoma	8
Hemangioma	6
Schwannoma	3
Neurofibroma	3
Myxoma	1
Myoepithelioma	1
Giant cell tumor of tendon sheet	1
Elastofibroma dorsi	1
Pigmented villonodular synovitis	1
Tumor-like structures	
Intramuscular hematoma	1
Crural abscess	1
Focal synovitis	1
Epidermal-type keratinous cyst	1
Myositis ossificans	1
Malignant (n=16)	
Malignant mesenchymal tumor	3
Synovial sarcoma	2
Liposarcoma	2
Leiomyosarcoma	2
Undifferentiated pleomorphic sarcoma	2
Pleomorphic malignant fibrous histiocytoma	1
Malignant giant cell tumor	1
Metastasis	3
İntermediate–borderline (n=5)	
Desmoid tumor	3
Fibromatosis	1
Angiomatous fibrous histiocytoma	1

The *K-trans* and *iAUC* values of malignant soft tissue lesions were found to be significantly higher statistically compared to those of the benign lesions ($P < .001$). Similarly, *Ve* values of the malignant tumors were found to be statistically significantly higher compared to those of the benign lesions ($P < .05$). There was no significant difference between malignant and benign lesion groups in terms of *Kep* values ($P > .05$) (Figure 1).

Table 2. The Demographic Characteristics of the Patients and the Lesion Dimensions by Group

	Benign (n=30)	Malignant (n=21)	*P*
Age	41 ± 17 (18-82)	44 ± 23 (13-84)	.674
Gender (male/female)	14/16	13/8	.288
Mean dimension (cm)	7.7 ± 4.7 (1.7-20)	9.0 ± 4.9 (2.5-24)	.224

Data: mean ± standard deviation.

Table 3. Distributions in the Benign and Malignant Lesion Groups According to the SIT Curve Categories

Type of the SIT Curves	Benign (n=30)	Malignant (n=21)
Type 1	9 (30.0%)	–
Type 2	10 (33.3%)	–
Type 3	6 (20.0%)	4 (19.0%)
Type 4	–	4 (19.0%)
Type 5	5 (16.7%)	13 (62.0%)

Receiver operating characteristic curve analysis demonstrated that when the cut-off point of *k-trans* was determined to be 0.111, the sensitivity was found to be 85.7%, the specificity was 73.3%, PPV was 69.2%, and NPV was 88.0% for differentiating between benign and malignant lesions. When the cut-off point for *Ve* was determined to be 0.406, the sensitivity was found to be 76.2%, the specificity was 70.0%, PPV was 64.0%, and NPV was 80.8% for differentiating between benign and malignant lesions. When the cut-off point for *iAUC* was determined to be 10.606, the sensitivity, specificity, PPV, and NPV were found to be similar to the values found for *k-trans* as 85.7%, 73.3%, 69.2%, and 88.0%, respectively (Figures 2 and 3).

There were significant differences between SIT curve types and the values of k-trans, Ve, and iAUC ($P < .001$). In terms of the k-trans, Ve, and iAUC values, no differences were found between the type 1 and 2 SIT curves representing the benign lesions, whereas individual differences with statistical significance were noted between the type 1 curve and each of the type 3, type 4, and type 5 curve representing the malignant lesions ($P < .05$). In addition, the Type 2 SIT curve was observed to be significantly higher in the benign group and the type 5 curves representing the malignant lesions in terms of k-trans, Ve, and iAUC values ($P < .05$). However, in terms of k-trans, Ve, and iAUC values, no significant differences were detected between the Type 2 SIT curves and type 3 and 4 SIT curves representing the malignant lesions ($P > .05$).

DISCUSSION

Dynamic contrast-enhanced MRI is based on the PWI technique, reflecting the functional condition of the tumoral vasculature indirectly. The pathological basis of perfusion is associated with the number of vessels in the tumor tissue and their functional modifications. In malignant tumors, the contrast agent diffuses into the extracellular space swiftly, and a fast staining of the tumor, as well as its washout, is observed. In contrast, in benign tumors, the vascular intensity is relatively lower and the infusion effect of the contrast agent is not significant. Used by Tofts, the two-compartment kinetic model (microvascular and extravascular interstitium) is commonly used during the DCE-MRI. The acquired results are analyzed, and the K-trans, kep, Ve, and iAUC values, which are the vascular function parameters, are found.[10]

Table 4. The Comparison of the Quantitative Perfusion Parameters at T1W Dynamic Perfusion MRI in Benign and Malignant Lesion Groups

	Benign (n=30)	95% CI	Malignant (n=16)	95% CI	*P*
K-trans	0.107 ± 0.120	0.062-0.151	0.250 ± 0.192	0.163-0.397	.000*
Kep	2.633 ± 3.718	1.244-4.021	0.826 ± 0.939	0.398-1.253	.628
Ve	0.294±0.294	0.184-0.403	0.515 ± 0.205	0.422-0.608	.004*
IUAC	8.096±9.008	4.732-11.459	18.874 ± 9.469	14.563-23.184	.000*

Data: nean ± standard deviation.

*$P < .05$.

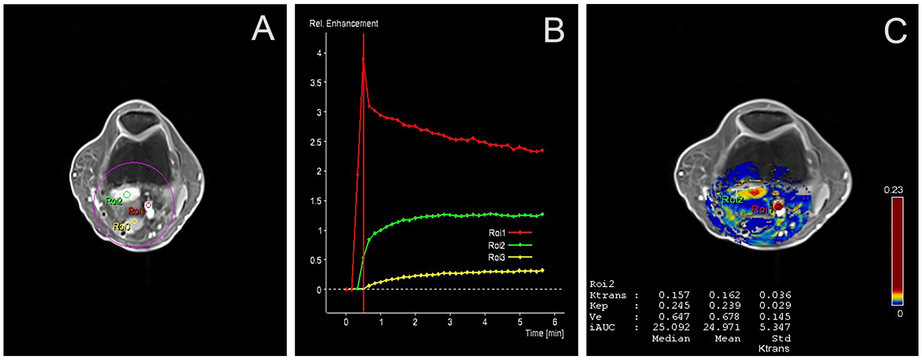

Figure 1. A 20-year-old-woman with a painful and locked knee. A soft tissue lesion with lobulated contours is present at the supracondylar level in the knee joint space posteromedially (A). The lesion demonstrates a type 3 curve (B), which is characterized by initial fast contrast enhancement followed by a plateau phase. On the parametric perfusion mapping of the lesion (C), K-trans, Kep, Ve, and iAUC values of 0.162, 0.239, 0.678, and 24.971, respectively, have been obtained. The k-trans, Ve, and iAUC values of this lesion have been found to be higher than the cut-off points for the differential diagnosis of benign and malignant lesions. The lesion has been diagnosed with pigmented villonodular synovitis histopathologically.

Costa et al[9] compared the diagnostic efficacy of proton MRI spectroscopy and DCE perfusion MRI investigations in 55 musculoskeletal tumor cases, consisting of 27 malignant and 28 benign cases. This study reported robust associations of the type 1-2 curves with benign lesions and of the Type 4 curves with malignant lesions. In addition, it was noted that Type 3 curves were not useful in differentiating benign and malignant lesions. In our study, all the lesions with Type 1 and 2 SIT curve patterns were in the benign group. We believe that this pattern is a reliable indicator of benign lesions. Similar to the above-mentioned study, the SIT curve Type 3 pattern was found in the benign and malignant groups at similar rates (20.0% and 19.0%, respectively) in our study. The Type 5 curve pattern was identified in 62% of the malignant cases and in 16% of the benign cases in our study, this pattern was found to be an important finding in the diagnosis of malignancies and

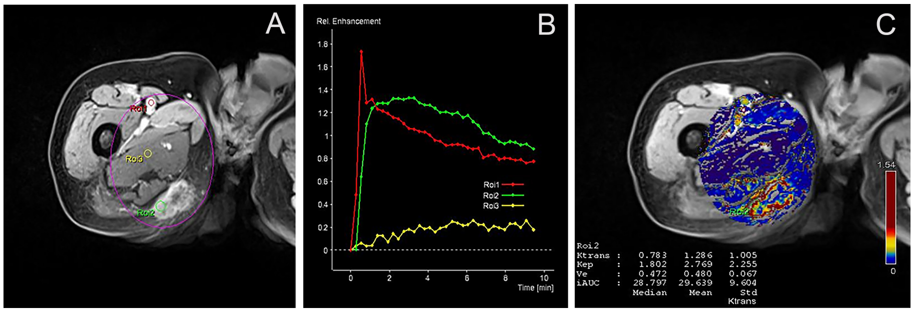

Figure 2. An 84-year-old male with a diagnosis of squamous cell malignant tumor of the lung with a mass located behind the femur. The lesion, with irregularly lobulated contours, is observed in the subcutaneous fat tissue of the right thigh posteriosuperiorly (A). The lesion demonstrates a type 4 curve, which is characterized by initial fast contrast enhancement followed by a wash-out phase (B). On the parametric perfusion mapping of the lesion (C), k-trans, kep, Ve, and iAUC values of 1.286, 2.769, 0.480, and 29.639 have been obtained, respectively. The k-trans, Ve, and iAUC values of this lesion have been found to be significantly higher than the cut-off points of these parameters for the differential diagnosis of benign and malignant lesions. The lesion has been diagnosed with metastasizing malignant neoplasm of the lung histopathologically.

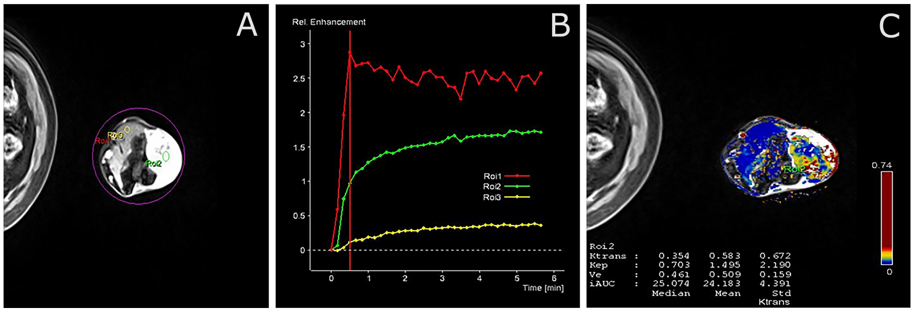

Figure 3. A 41-year-old male with a soft tissue mass in the left elbow. The soft tissue mass, with irregularly lobulated contours, is present in the left elbow posteriorly in the skin and subcutaneous tissue (A). The lesion demonstrates a Type 5 curve (B). On the parametric perfusion mapping of the lesion (C), the following k-trans, kep, Ve, and iAUC values of 0.583, 1.495, 0.509, and 24.183 have been obtained. The k-trans, Ve, and iAUC values of this lesion have been found to be significantly higher than the cut-off points for the differential diagnosis of benign and malignant lesions. A high-grade malignant mesenchymal tumor has been the histopathological diagnosis.

in deciding biopsy procedures. However, it is not considered to be a reliable indicator individually when used alone.

Van Rijswijk et al[11] reported that the demonstration of a plateau or wash-out phase following early and intense contrast enhancement (SIT curves Type 3 and 4) in soft tissue tumors supported the diagnosis of malignant tumors. Van der Woude et al[13] found that SIT curve typing had 86% sensitivity and 81% specificity for differentiating malignant from benign tumors from each other by demonstrating the progression of contrast enhancement. However, they did not observe a statistically significant difference using this method for the differential diagnosis of bone tumors. In our study, all of the 4 cases with SIT curve Type 4 patterns were in the malignant group, whereas the Type 3 pattern was found at similar rates in both the benign and malignant lesion groups (20.0% and 19.0%, respectively) in our study. The Type 3 pattern was not found to be reliable for differential diagnosis.

The study by Yao et al[12] compared the microvascular intensities using DCE-MRI in 26 histopathologically proven rectal cancer cases. They calculated the following parameters: k-trans, kep, and Ve. They found that the values of these parameters were significantly higher in the tumoral tissue compared to those values found in the normal rectal wall. The study reported that k-trans values were positively correlated with Duke and TNM stagings, serosal involvement, and lymphatic metastases to a moderate to high extent; however, kep values were reported to demonstrate a moderate degree of correlation. No correlations were found with the Ve values. In our study as well, the k-trans values were observed to be significantly higher in the malignant lesion group of soft tissue tumors.

A study by Jackson et al[14] compared histopathologically proven prostate cancer lesions in 18 patients by DCE-MRI pharmacokinetic parameters and T2W image findings, aiming to identify a malignant lesion located at each pixel. The sensitivity and specificity of DCE-MRI to diagnose the lesions were found to be 50% and 85%, respectively. For the T2W images, the sensitivity was 21% and the specificity was 89%. When the authors compared the DCE-MRI parameters, namely, the k-trans, kep, and Ve values found for the cancer tissue in the prostate gland, they found these values significantly higher compared to those obtained in the benign peripheral zone. Finally, the authors reported that DCE-MRI was superior to the T2W section images in determining the locations of the lesions in prostate cancers.

Ma et al[10] investigated the efficacy of the T1W imaging by dynamic perfusion MRI in a total of 44 breast lesions. Of these lesions, 30 were malignant lesions. The authors reported that k-trans, kep, and iAUC values were found to be statistically significantly different in differentiating malignant and benign lesions from each other, while the Ve values were not statistically significant. The non-significantly different Ve values, representing the contrast agent percentages in the tissue spaces, were associated with the increased k-trans and kep values due to the increased neovascular permeability in the malignant lesions. Therefore, according to the "Ve=k-trans/kep" formula, they explained that the Ve values did not show any differentiation. In contrast to the findings of the study described above, Ve values in our study were found to be statistically significantly different in differentiating malignant and benign lesions. We believe that this result may be associated with the statistically significantly different k-trans values and with the non-significant differences found with the kep values.

In 36 breast cancer cases, Li et al[15] compared the pathological response to the first cycle of neoadjuvant chemotherapy by comparing the tumor sizes, DCE-MRI, apparent diffusion coefficient (ADC) values acquired by the diffusion-weighted imaging (DWI) and the kep/ADC ratios. Consequently, they reported that the kep/ADC ratio was more statistically significant. They reported that the area under the curve (AUC) for the kep/ADC was 0.88, superior to kep (AUC: 0.76) and ADC (AUC: 0.82) values in predicting the pathological response after chemotherapy. They suggested that the combined use of DCE-MRI and DWI might be beneficial in evaluating the response to chemotherapy and in assessing treatment results during follow-ups in cases with breast cancer. On the other hand, in our study, the kep parameter was not found to be useful in differentiating benign and malignant soft tissue lesions from each other. We suggest that this finding might be associated with the heterogeneous microvascular intensity found in soft tissue tumors.

Baik et al[16] investigated the efficacy of the tissue permeability factor acquired by the DCE-MRI in differentiating between benign and malignant pulmonary lesions in 30 cases of pulmonary lesions. They evaluated the k-trans, kep, and Ve parameters as the tissue permeability factors. Their study reported that the perfusion parameter of k-trans acquired by the DCE-MRI might be beneficial in determining whether the pulmonary nodules or masses were benign or malignant. Similarly, in the differential diagnosis, our study determined the k-trans value to be the most beneficial parameter together with the iAUC values.

The limitations of our study might include the relatively insufficient number of cases and their variabilities, as well as the unavailability of the histopathological diagnoses for some cases. Perfusion parameters may be affected by tumor grade. The lack of tumor stages is another limitation of this study. We conclude that further studies should be conducted with larger sample sizes and more variable cases to better demonstrate the efficacy of the DCE-MRI perfusion parameters in differentiating malignant from benign soft tissue tumors.

In conclusion, our study showed that the quantitative perfusion parameters and the contrast-enhanced curve types acquired by the DCE-MRI provided useful contributions to the diagnosis in determining whether the soft tissue lesions were benign or malignant. We suggest that further studies in broader patient groups with more diagnostic variability should be conducted to better demonstrate the efficacy of this technique in the malignant versus benign differentiation of soft tissue tumors.

Availability of Data and Materials: The datasets used and/or analysed during the current study are available from the corresponding author on reasonable request.

Ethics Committee Approval: Ethical approval was received from the local Ethics Committee of Gazi University Faculty of Medicine, approval number 513, date november 11, 2014.

Informed Consent: N/A.

Peer-review: Externally peer-reviewed.

Author Contributions: Concept – I.O., M.F.O.; Design – I.O., M.F.O., N.T., M.U.; Supervision – N.T., M.U., F.D.G.; Resources – N.T., M.U.; Materials – N.T., M.U.; Data Collection and/or Processing – I.O.; Analysis and/or Interpretation – I.O., N.T., M.U.; Literature Search – I.O., M.F.O.; Writing Manuscript – I.O., M.F.O.; Critical Review – I.O., M.F.O., N.T., M.U.

Declaration of Interests: The authors have no conflict of interest to declare.

Funding: The authors declared that this study has received no financial support.

REFERENCES

1. Tuncbilek N, Karakas HM, Okten OO. Dynamic contrast enhanced MRI in the differential diagnosis of soft tissue tumors. *Eur J Radiol*. 2005;53(3):500-505. [CrossRef]
2. De Schepper A, Parizel P, Ramon F, De Beuckeleer L, Vandevenne J. *Imaging of Soft Tissue Tumors. New York*. Springer, Berlin; 1997.
3. Hough TJ, Tung GA, Terek RM. Staging, characterization, and grading. In: De S, Parizel PA, Ramon F, et al., eds. *Imaging of Soft Tissue Tumors*. Berlin, Heidelberg: Springer; 1997:113-125.
4. Kransdorf MJ, Murphey MD. *Imaging of Soft Tissue Tumors*. Philadelphia: WB Saunders; 1997.
5. Petasnick JP, Turner DA, Charters JR, Gitelis S, Zacharias CE. Soft-tissue masses of the locomotor system: comparison of MR imaging with CT. *Radiology*. 1986;160(1):125-133. [CrossRef]
6. Aisen AM, Martel W, Braunstein EM, McMillin KI, Phillips WA, Kling TF. MRI and CT evaluation of primary bone and soft-tissue tumors. *AJR Am J Roentgenol*. 1986;146(4):749-756. [CrossRef]
7. Paldino MJ, Barboriak DP. Fundamentals of quantitative dynamic contrast-enhanced MR imaging. *Magn Reson Imaging Clin N Am*. 2009;17(2):277-289. [CrossRef]
8. Park MY, Jee WH, Kim SK, Lee SY, Jung JY. Preliminary experience using dynamic MRI at 3.0 Tesla for evaluation of soft tissue tumors. *Korean J Radiol*. 2013;14(1):102-109. [CrossRef]
9. Costa FM, Vianna EM, Domingues RC, et al. Espectroscopia de prótons e perfusão por ressonância magnética na avaliação dos tumores do sistema musculoesquelético. *Radiol Bras*. 2009;42(4):215-223. [CrossRef]
10. MA ZS, WANG DW, SUN XB, et al. Quantitative analysis of 3-Tesla magnetic resonance imaging in the differential diagnosis of breast lesions. *Exp Ther Med*. 2015;9(3):913-918. [CrossRef]
11. van Rijswijk CSP, Geirnaerdt MJA, Hogendoorn PCW, et al. Soft-tissue tumors: Value of static and dynamic gadopentetate dimeglumine-enhanced MR imaging in prediction of malignancy. *Radiology*. 2004;233(2):493-502. [CrossRef]
12. Yao WW, Zhang H, Ding B, et al. Rectal cancer: 3D dynamic contrast-enhanced MRI; correlation with microvascular density and clinicopathological features. *Radiol Med*. 2011;116(3):366-374. [CrossRef]
13. van der Woude HJ, Verstraete KL, Hogendoorn PC, Taminiau AH, Hermans J, Bloem JL. Musculoskeletal tumors: does fast dynamic contrast-enhanced subtraction MR imaging contribute to the characterization? *Radiology*. 1998;208(3):821-828. [CrossRef]
14. JACKSON ASN, REINSBERG SA, SOHAIB SA, et al. Dynamic contrast-enhanced MRI for prostate cancer localization. *Br J Radiol*. 2009;82(974):148-156. [CrossRef]
15. Li X, Abramson RG, Arlinghaus LR, et al. Multiparametric magnetic resonance imaging for predicting pathological response after the first cycle of neoadjuvant chemotherapy in breast cancer. *Invest Radiol*. 2015;50(4):195-204. [CrossRef]
16. Baik SH, Jin GY, Han YM, Lee YC, Kwon KS. Usefulness of tissue permeability factor in differentiating benign and malignant pulmonary lesions on dynamic contrast-enhanced MRI. *J Korean Soc Radiol*. 2013;69(1):57. [CrossRef]

Current Research in MRI
Original Article

Comparison of Digital Subtraction Angiography and Non-Contrast-Enhanced Magnetic Resonance Angiography Findings in Imaging Carotid Arteries

Kemal Bugra Memis[1], Ali Osman Gulmez[1], Umman Sanlıdilek[2]

[1]Department of Radiology, Erzincan Binali Yıldırım University Faculty of Medicine, Erzincan, Türkiye
[2]Department of Radiology, Ankara University Faculty of Medicine, Ankara, Türkiye

Cite this article as: Memis KB, Gulmez AO, Sanlıdilek U. Comparison of digital subtraction angiography and non-contrast-enhanced magnetic resonance angiography findings in imaging carotid arteries. *Current Research in MRI*, 2024;3(2):49-56.

Corresponding author: Kemal Bugra Memis, e-mail: kemalbugramemis@gmail.com

Received: May 28, 2024 **Revision requested:** August 5, 2024 **Last revision received:** August 15, 2024 **Accepted:** August 16, 2024
Publication Date: August 27, 2024

DOI:10.5152/CurrResMRI.2024.24097

Abstract

Objective: This study aimed to compare the diagnostic effectiveness and precision of non-contrast magnetic resonance angiography (MRA) with the most reliable digital subtraction angiography (DSA) findings in imaging the cervical segment of the carotid arteries.
Methods: From January 2012 to April 2018, a retrospective evaluation was conducted on the images of 23 patients who had undergone DSA and non-contrast MRA for the carotid arteries in the neck. The evaluation was based on data retrieved from the local database. The stenosis rates were categorized as follows: normal, stenosis less than 50%, stenosis between 50% and 69%, stenosis equal to or greater than 70%, and total occlusion.
Results: Out of the 23 participants who were included in the study, 13 (56.5%) were female and 10 (43.5%) were male. The average age of the patients was 58.5, with a range of 29 to 84 and a median value of 60. The non-contrast MRA examination had a sensitivity of 78%, specificity of 97%, positive predictive value of 88%, negative predictive value of 95%, and diagnostic accuracy of 93% for detecting significant stenosis (>50%) in the internal carotid artery (ICA), as determined by the gold standard DSA. The non-contrast MRA had a sensitivity of 86%, specificity of 100%, positive predictive value of 100%, negative predictive value of 98%, and a diagnostic accuracy rate of 98%.
Conclusion: Non-contrast MRA imaging is a secure technique for identifying atherosclerotic carotid artery disease with a high level of accuracy and precision.
Keywords: Digital subtraction angiography, extracranial carotid arteries, non-contrast MR angiography

INTRODUCTION

Cerebrovascular disease, such as strokes, is a leading cause of mortality in developed nations. The occurrence results from either hemodynamic or, more commonly, atheroembolic mechanisms, which are caused by atherosclerotic plaques of the carotid bifurcation in approximately 15%-20% of cases.[1] Given that plaques in the extracranial carotid arteries are responsible for 25% of ischemic cerebrovascular events that result in chronic neurological deficiencies, it is crucial to prioritize the treatment of these abnormalities.[2] Options for treatment consist of endarterectomy or percutaneous transluminal carotid angioplasty and stenting, which is a radiological procedure performed by interventional means. Medical interventions for mitigating risk factors are also encompassed. Accurate and precise measurement of the extent of stenosis is crucial in selecting the suitable treatment.[3]

Digital subtraction angiography (DSA) is considered the most reliable method for imaging the carotid arteries. However, noninvasive imaging techniques like magnetic resonance angiography (MRA), computed tomographic angiography (CTA), and color Doppler ultrasonography (CDUS) also have a significant role in evaluating the carotid arteries.[4]

Color Doppler ultrasonography, a readily available and minimally invasive procedure, is frequently employed as the initial diagnostic imaging technique for screening carotid artery stenosis. However, the outcome is greatly influenced by the user's level of expertise and proficiency. Digital subtraction angiography, which is considered the standard for determining the severity of narrowing in blood vessels and the characteristics of plaque, is not universally applicable to all patients due to the associated hazards and expenses. Currently, non-invasive techniques such as CTA and MRA are becoming more commonly utilized for diagnosing carotid stenosis, replacing the need for invasive DSA.[3] Computed tomographic angiography is the primary diagnostic technique for imaging blood vessels in cases of sudden stroke.[5] Nevertheless, it is important to note that the procedure involves ionizing radiation, and the intravenous contrast material utilized can cause allergic reactions and have nephrotoxicity effects.

Furthermore, MRA is both noninvasive and spared from ionizing radiation. Currently, the most common method for imaging the carotid arteries is through the use of contrast-enhanced MRA. This involves injecting gadolinium-based contrast agents via an intravenous route. Magnetic resonance imaging contrast agents have minimal adverse effects; however, they can induce nephrogenic systemic fibrosis in individuals with renal insufficiency. The awareness of this potential side effect and the existence of patients who are unable to undergo contrast administration for various reasons have resulted in a growing interest in non-contrast MRA in recent times. The prevailing non-contrast MRA technique that is frequently utilized is known as "time-of-flight" (TOF) angiography.[4] The primary constraints of MRA are motion artifacts caused by patient noncompliance and intolerance in individuals experiencing acute stroke. Furthermore, it is contraindicated in patients with pacemakers and certain magnetic devices.[5,6]

The purpose of this study was to compare the results of non-contrast MRA and DSA, which is considered the most reliable method in our center, for imaging the cervical segments of carotid arteries. Additionally, we aimed to assess the diagnostic efficiency and accuracy of the non-contrast MRA technique.

MATERIAL AND METHODS

The study was initiated with the approval of the Ankara University Faculty of Medicine Clinical Research Ethics Committee (Date: 2014, Decision No: 06-355-18). All patients provided written informed consent for the publication of this article using their data.

A retrospective analysis was conducted on 29 patients who underwent both DSA and non-contrast MRA scans for carotid arteries at our hospital between January 2012 and April 2018. Initially, 4 patients were excluded from the study because more than 1 year had passed between the 2 examinations. In addition, we excluded 2 patients from the study because their images were affected by motion artifacts in MRA and artifacts caused by stents in the carotid arteries. For the remaining 23 cases, the carotid arteries in the neck were divided into the right and left common carotid artery (CCA), internal carotid artery (ICA), and external carotid artery (ECA). These arteries were then assessed individually using both methods from the PACS database. An experienced radiologist evaluated the existing images without knowledge of the patients' clinical data. The DSA images were evaluated separately from the initial evaluation, which took place 4 weeks after the MRA images were evaluated initially. Subsequently, this assessment procedure was reiterated once again at 4-week intervals. Stenosis rates were determined using the North American Symptomatic Carotid Endarterectomy Trial (NASCET) criteria and categorized as "normal," "<50% stenosis," "50%-69% stenosis," "≥70% stenosis," and total occlusion.

MAIN POINTS

- Non-invasive non-contrast MRA can be used as an alternative to DSA, an invasive method, for diagnosing atherosclerotic carotid artery disease, even though DSA is considered the gold standard.
- Non-contrast MRA can be utilized as an adjunct imaging technique in patients with impaired renal function, particularly when CDUS is insufficient in visualizing the carotid arteries. This method does not necessitate the use of nephrotoxic agents.
- Non-contrast MRA is more useful in populations that are averse to ionizing radiation.

All non-contrast MRA examinations were obtained with the time of flight (TOF) angiography technique. Fifteen of these scans were conducted using a 3.0 T magnetic resonance imaging (MRI) scanner (Siemens Magnetom Verio, Erlangen, Germany), while 8 were performed using a 1.5 T MRI scanner (Siemens Magnetom Aera, Erlangen, Germany). The acquisition parameters in the axial 3D TOF MRA examination performed with a 3.0 T device were determined as TR 21 ms, TE 3.6 ms, deviation angle 25 degrees, slice thickness 1 mm, matrix 384 × 312, FOV 20 × 16 cm. The acquisition parameters in the axial 3D TOF MRA examination performed with a 1.5 T device were determined as TR 24 ms, TE 7.2 ms, deviation angle 20 degrees, section thickness 0.8-1 mm, matrix 512 × 512, FOV 20 × 16 cm.

The DSA techniques were executed using an Artis Zee (Siemens Healthcare, Erlangen, Germany) angiography device. The patients underwent the procedure without the administration of sedation. Following the application of povidone-iodine solution for local field sterilization, the femoral artery was utilized as the access route after the application of dressing and local anesthesia. Following the puncture using the Seldinger method, a 5-French sheath was inserted into the femoral artery. The pigtail angiography catheter was inserted through the sheath and used to visualize the aortic arch and its branches. The carotid artery exits were identified based on the images, and subsequently, a Simmons type II catheter was used to selectively catheterize the carotid arteries after replacing the catheter. Next, conventional images of the carotid arteries were acquired in anteroposterior, lateral, and oblique orientations for both the right and left sides. During the examination, the patient received a suitable dose of nonionic contrast material based on their weight, with a maximum limit of 100 mL, using an automatic pump injector.

The stenoses were assessed on both DSA and MRA images using the NASCET criteria (stenosis = [1 -–minimal residual lumen/distal vascular lumen diameter] × 100%). During the DSA method, the degree of stenosis in the carotid arteries was assessed by measuring the percentage of narrowing. This measurement was taken from all projections that provided a clear view of the carotid arteries without any overlapping blood vessels. The most severe narrowing of the artery was chosen, and its representation was recorded. The main datasets of 3D TOF and maximum intensity projection (MIP) images were examined. The degree of stenosis in the carotid arteries was assessed using sagittal and coronal MIP images, and the most severe degree of stenosis was recorded. When the presence of occlusion was suspected in 3D TOF MIP images, the potential occurrence of slow flow was ruled out by assessing 2D TOF images. If there was no detected blood flow in the expected pathway beyond the examined artery, the vessel was classified as totally obstructed. The assessment of the image was conducted using the Syngo MR software (Siemens Medical Solutions, Erlangen, Germany) on a workstation.

The gold standard for detecting carotid artery stenosis was accepted as DSA. Sensitivity, specificity, positive predictive value (PPV), and negative predictive value (NPV) were calculated for the non-contrast MRA examination. Furthermore, observer agreement was assessed using the kappa correlation test. The provided information includes the mean ± SD for numerical variables, the minimum and maximum values (min-max), and the number and percentage values for categorical variables. The relationship between the features was analyzed at the qualitative measurement level using either Fisher's exact test or Pearson's chi-square test. The statistical analysis was conducted using the SPSS 25.0 software (IBM SPSS Corp.;

Armonk, NY, USA). Statistical significance was determined by a *P*-value threshold of less than .05.

RESULTS

Out of the total of 23 participants who were part of the research, 13 (56.5%) were female and 10 (43.5%) were male. The average age of the patients was determined to be 58.5, with a range of 29 to 84 and a median value of 60.

The stenosis rates detected in the first and second evaluations using both examination methods of the carotid arteries examined in the cases are shown in Tables 1 and 2, respectively.

When the cases with and without significant stenosis (over 50%) compared to NASCET in both ICAs in non-contrast MRA and DSA examinations are evaluated, the findings are shown in the tables below (Tables 3 and 4). The sensitivity was 78%, specificity 97%, positive predictive value 88%, negative predictive value 95%, and diagnostic accuracy 93% for detecting significant stenosis (>50%) of ICA for non-enhanced MRA examination according to the gold standard DSA.

When the cases with and without critical stenosis (over 70%) according to NASCET in both ICAs in non-contrast MRA and DSA examinations are evaluated, the findings are shown in the tables below (Tables 5 and 6). The sensitivity was 86%, specificity 100%, positive predictive value 100%, negative predictive value 98%, and diagnostic accuracy 98% for detecting critical stenosis (>70%) of ICA for non-enhanced MRA examination according to the gold standard DSA.

There was no significant stenosis in the right CCA and ECA, and there was 1 case with significant stenosis in the left CCA and ECA.

The agreement and kappa values between the results of the first and second evaluation of the carotid arteries according to the kappa agreement analysis are shown in the table below (Table 7). Accordingly, it was determined that the agreement between the 2 measurement sets was significant.

DISCUSSION

Cerebrovascular events are a leading cause of mortality in developed nations. Ischemic strokes account for about 85% of all strokes. Extracranial carotid atherosclerosis accounts for 20% of these cases.[7,8] Given that atherosclerotic plaques in the extracranial carotid arteries are responsible for 25% of ischemic cerebrovascular events resulting in permanent neurological deficits, it is crucial to prioritize the treatment of these lesions.[2] Based on data from the Framingham heart study,[9] it was found that 7% of women and 9% of men aged 66-93 had carotid stenosis with a degree of more than 50%. Another study found that even carotid plaques that were subclinical and hemodynamically stable in individuals aged 45-64 were indicative of future cerebrovascular events. The NASCET study[10] found a correlation between the severity of stenosis and the likelihood of stroke development in symptomatic patients. The annual risk of ipsilateral stroke is 4.4% in cases where carotid stenosis is between 50 and 69% and the patient is treated conservatively. However, this risk increases to 13% in patients with stenosis above 70%. For patients without symptoms, the likelihood of having a stroke within a year is less than 1% when receiving aggressive medical treatment, provided that the narrowing of the blood vessels is greater than 50%. These studies indicate that it is necessary to use diagnostic methods to screen patients with risk factors for asymptomatic atherosclerotic carotid disease, as treatment can effectively reduce the risk of stroke. Therefore, by promptly identifying and treating the condition, the patient's yearly

Table 1. Right and Left CCA, ICA, ECA Stenosis Rates in First Measurement (%)

		Right CCA		Right ICA		Right ECA		Left CCA		Left ICA		Left ECA	
Patient No	**Age/Gender**	**MRA**	**DSA**	**MRA**	**DSA**	**MRA**	**DSA**	**MRA**	**DSA**	**MRA**	**DSA**	**MRA**	**DSA**
1	29/F	N	N	N	N	N	N	100	100	100	100	100	100
2	77/M	N	N	<50	<50	N	N	N	N	>70	>70	N	N
3	47/M	N	N	<50	N	N	N	N	N	<50	N	N	N
4	60/F	N	N	<50	50-69	<50	<50	N	N	100	100	<50	<50
5	80/F	N	N	N	N	N	N	N	N	N	N	N	N
6	34/M	N	N	<50	<50	N	N	N	N	<50	<50	N	N
7	70/F	N	N	N	N	N	N	N	N	<50	<50	N	N
8	66/M	<50	<50	<50	<50	<50	<50	<50	<50	50-69	<50	N	N
9	43/F	N	N	N	N	N	N	N	N	N	N	N	N
10	72/F	<50	<50	N	N	N	N	N	N	N	N	N	N
11	64/M	N	N	N	N	<50	<50	N	N	>70	>70	N	N
12	50/F	N	N	N	N	N	N	N	N	N	N	N	N
13	60/M	<50	<50	<50	50-69	N	N	<50	<50	N	N	N	N
14	70/M	N	N	<50	<50	N	N	N	N	>70	>70	N	N
15	44/F	N	N	N	N	N	N	N	N	N	N	N	N
16	50/F	N	N	N	N	N	N	N	N	N	N	N	N
17	84/M	N	N	>70	>70	N	N	<50	<50	<50	<50	<50	N
18	62/F	N	N	N	N	<50	<50	N	N	N	N	N	N
19	78/F	N	N	N	N	<50	50-69	<50	<50	N	N	N	N
20	52/M	N	N	N	N	N	N	N	N	N	N	N	N
21	50/F	N	N	N	N	N	N	N	N	N	N	N	N
22	34/F	N	N	N	N	N	N	N	N	N	N	N	N
23	70/M	N	N	50-69	>70	<50	<50	<50	<50	<50	<50	<50	<50

CCA, common carotid artery; ECA, external carotid artery; F, female; ICA, internal carotid artery; M, male.

Table 2. Right and Left CCA, ICA, ECA Stenosis Rates in Second Measurement (%)

		Right CCA		Right ICA		Right ECA		Left CCA		Left ICA		Left ECA	
Patient No	**Age/Gender**	**MRA**	**DSA**	**MRA**	**DSA**	**MRA**	**DSA**	**MRA**	**DSA**	**MRA**	**DSA**	**MRA**	**DSA**
1	29/F	N	N	N	N	N	N	100	100	100	100	100	100
2	77/M	N	N	<50	<50	N	N	N	N	>70	>70	N	N
3	47/M	N	N	N	N	N	N	N	N	N	N	N	N
4	60/F	N	N	<50	50-69	<50	<50	N	N	100	100	<50	<50
5	80/F	N	N	N	N	N	N	N	N	N	N	N	N
6	34/M	N	N	<50	<50	N	N	N	N	<50	<50	N	N
7	70/F	N	N	N	N	N	N	N	N	<50	<50	N	N
8	66/M	<50	<50	<50	<50	<50	<50	<50	<50	50-69	<50	N	N
9	43/F	N	N	N	N	N	N	N	N	N	N	N	N
10	72/F	<50	<50	N	N	N	N	N	N	N	N	N	N
11	64/M	N	N	N	N	<50	<50	N	N	>70	>70	N	N
12	50/F	N	N	N	N	N	N	N	N	N	N	N	N
13	60/M	<50	<50	<50	50-69	N	N	<50	<50	N	N	N	N
14	70/M	N	N	<50	<50	N	N	N	N	>70	>70	N	N
15	44/F	N	N	N	N	N	N	N	N	N	N	N	N
16	50/F	N	N	N	N	N	N	N	N	N	N	N	N
17	84/M	N	N	>70	>70	N	N	<50	<50	<50	<50	<50	N
18	62/F	N	N	N	N	<50	<50	N	N	N	N	N	N
19	78/F	N	N	N	N	<50	50-69	<50	<50	N	N	N	N
20	52/M	N	N	N	N	N	N	N	N	N	N	N	N
21	50/F	N	N	N	N	N	N	N	N	N	N	N	N
22	34/F	N	N	N	N	N	N	N	N	N	N	N	N
23	70/M	N	N	50-69	>70	<50	<50	<50	<50	<50	<50	<50	<50

CCA, common carotid artery; ECA, external carotid artery; F, female; ICA, internal carotid artery; M, male.

likelihood of experiencing a stroke can be diminished. Treatment options encompass surgical endarterectomy, percutaneous transluminal carotid angioplasty, and stenting, which is an interventional radiological procedure. Additionally, medical treatments targeting risk factors are also considered. Furthermore, obtaining precise and accurate measurements of the extent of stenosis is crucial in determining the most suitable course of treatment.[11] Medical treatment is adequate for stenosis below 50%. However, for stenosis ranging from 50% to 69%, it is recommended to undergo medical treatment and have follow-up appointments every 6 months. In cases where there is a narrowing of 70% or more in the carotid artery and the patient is experiencing symptoms, surgical endarterectomy or percutaneous transluminal carotid angioplasty and stenting procedures are performed (Figures 1-4). However, surgical treatment is not appropriate in cases of occlusion.[12]

Digital subtraction angiography is still considered the gold standard for imaging the carotid arteries. However, DSA, which is an invasive method, has disadvantages such as containing ionizing radiation, the use of nephrotoxic agents, limited imaging projection, and a relatively high complication rate if not performed by qualified personnel. Embolism from a plaque potentially causing a cerebrovascular accident is one of its well-proven complications. The ACAS study reported a 1.2% risk of neurological deficit or death after DSA, while the NASCET study reported a 0.7% risk of permanent neurological deficit or death associated with selective angiography. The high complication rate limits its use as a screening test. In contrast, neither MRA nor CDUS carries the risk of complications at these rates. In addition, besides being noninvasive, they do not contain ionizing radiation. Currently, MRA imaging of the extracranial carotid arteries is mostly performed as contrast-enhanced angiography after the intravenous injection of gadolinium-based contrast agents. MR contrast agents have very few side effects, but they can cause nephrogenic systemic fibrosis in patients with renal failure. The fact that this possible side effect is now better known and the presence of patients who cannot receive contrast for other reasons has led to an increased

Table 3. Cases With and Without Significant Stenosis in MRA and DSA Examinations in the Right ICA

		DSA		
		There is Significant Narrowness	**No Significant Narrowing**	**Total**
MRA	There is significant narrowness	2	0	2
	No significant narrowing	2	19	21
	Total	4	19	23

DSA, digital subtraction angiography; ICA, internal carotid artery; MRA, magnetic resonance angiography.

Table 4. Cases With and Without Significant Stenosis in MRA and DSA Examinations in the Left ICA

		DSA		
		There is Significant Narrowness	**No Significant Narrowing**	**Total**
MRA	There is significant narrowness	5	1	6
	No significant narrowing	0	17	17
	Total	5	18	23

DSA, digital subtraction angiography; ICA, internal carotid artery; MRA, magnetic resonance angiography.

Table 5. Cases With and Without Critical Stenosis in MRA and DSA Examinations of the Right ICA

		DSA		
		There is Critical Stenosis	No Critical Stenosis	Total
MRA	There is critical stenosis	1	0	1
	No critical stenosis	1	21	22
	Total	2	21	23

DSA, digital subtraction angiography; ICA, internal carotid artery; MRA, magnetic resonance angiography.

Table 7. According to Kappa Analysis, Agreement Between the Results of the First and Second Evaluation of the Carotid Arteries and Kappa Values

Carotid Artery	Kappa Value	*P*
Right CCA	1.000	<.001
Right ICA	0.916	<.001
Right ECA	1.000	<.001
Left CCA	1.000	<.001
Left ICA	0.916	<.001
Left ECA	1.000	<.001

CCA, common carotid artery; ECA, external carotid artery; ICA, internal carotid artery.

interest in non-contrast MRA in recent years.[4,13,14] The most important difference of non-contrast MRA from RDUS, which is a cheaper and easily accessible noninvasive method, is that it is not user dependent. However, the most important disadvantage of TOF MRA, which is the most widely used non-contrast MRA method in carotid artery imaging today, is signal loss. Signal loss occurs due to the phase shift that develops due to the disruption of normal laminar flow in the vessel (turbulent flow pattern occurs near the stenotic plaque) and overstates the existing stenosis.[15,16] This may lead to incorrect diagnosis and treatment of the patient. In one of our patients in this study, left ICA stenosis was overestimated with TOF MRA, and the stenosis rate of less than 50% was measured between 50 and 69%. In addition, right ICA stenosis was underestimated by TOF MRA in 3 of our patients. While stenosis was between 50 and 69% in 2 of them, it was measured as less than 50%, and in one of them, the true stenosis rate was measured between 50 and 69%. In the last case, if the patient had not undergone DSA examination, surgical or interventional radiological treatment, which was actually indicated, would have been delayed.

In order for non-contrast MRA to be a diagnostic test that can be used in screening, the sensitivity, specificity rates, and positive and negative predictive values in detecting pathology should be known and at an acceptable level.

Chappell et al[13] stated that noninvasive test combinations do not increase sensitivity and specificity but increase the cost. The sensitivity values of all modalities in detecting stenosis between 50 and 69% were found to be significantly lower than their sensitivities in detecting stenosis between 70 and 99%. Therefore, they emphasized that it is difficult to detect moderate (50-69%) stenosis (since all modalities have low sensitivity values), but their diagnosis is important (because some patients in this group benefit from carotid endarterectomy). In our study, it was observed that the sensitivity and specificity values, which were found to be higher in stenosis above 70%, were consistent with the literature.

Table 6. Cases With and Without Critical Stenosis on MRA and DSA Examinations of the Left ICA

		DSA		
		There is Critical Stenosis	No Critical Stenosis	Total
MRA	There is critical stenosis	5	0	5
	No critical stenosis	0	18	18
	Total	5	18	23

DSA, digital subtraction angiography; ICA, internal carotid artery; MRA, magnetic resonance angiography.

Wardlaw et al[14] stated that the sensitivity of non-contrast MRA was 88% and the specificity was 84% in cases of critical stenosis of 70% and above. In stenosis of 50%-69%, the sensitivity of non-contrast MRA was 37%, and the specificity was 91%. In our study, the sensitivity was 86% and the specificity was 100% in detecting critical stenosis (>70%) of the ICA for non-contrast MRA examination. At this point, although our sensitivity values were similar to those in the study by Chappell et al and Wardlaw et al, our specificity values were slightly higher.

The utilization of a 3 T MRI system to acquire the majority of our 3D TOF MRA images represents a noteworthy advantage in our study. The limitations commonly discussed in the literature regarding 1.5 T MRI systems have been mostly eliminated. 3D TOF MRA benefits at 3 T MRI systems from both an improved signal-to-noise ratio (SNR) and longer T1 relaxation times in the cerebral parenchyma. This leads to enhanced saturation of stationary spins and improved contrast between

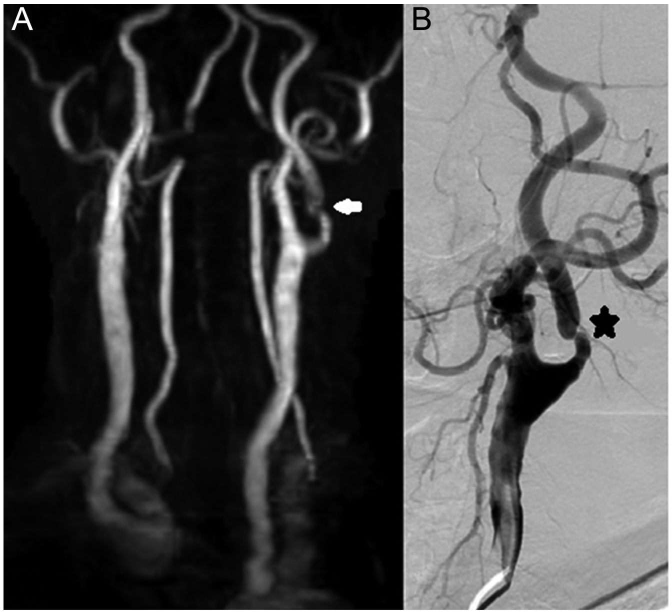

Figure 1. A 64-year-old male patient. He was admitted to our hospital with the complaint of abrupt onset of right upper and lower extremity weakness 3 months ago. He has a history of surgery due to hypertension, diabetes, and nephrolithiasis, and his creatinine value was found to be 1.4 in laboratory tests. The patient underwent carotid and vertebral artery RDUS, neck TOF MRA, and carotid DSA procedures in our unit, and then the patient was treated endovascularly. (A) A critical stenosis of over 70% is seen in the left ICA in the TOF MRA coronal MIP image (white arrow). (B) On DSA examination, more than 70% critical stenosis is observed in the left proximal ICA (black star).

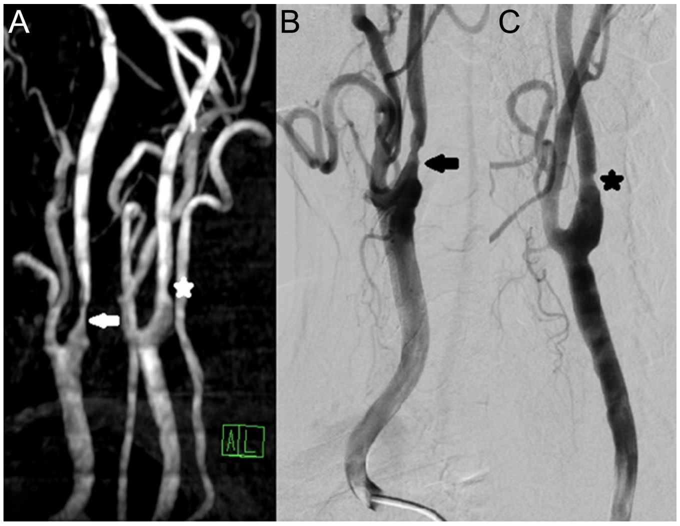

Figure 2. An 84-year-old male patient. He was admitted to our hospital with the complaint of weakness in the left upper extremity that developed 1 week ago. He has a history of hypertension, smoking, and an operation due to benign prostatic hyperplasia, and creatinine value was found to be 1.2 in laboratory tests. The patient underwent neck TOF MRA, and carotid DSA procedures in our unit. (A) On TOF MRA coronal-oblique MIP image, critical stenosis of over 70% (white arrow) in the right ICA and less than 50% stenosis in the left ICA (white star). (B) A critical stenosis of over 70% is observed in the proximal right ICA on DSA examination (black arrow). (C) Less than 50% stenosis is observed in the proximal left ICA on DSA examination (black star).

vessels and the background. High-spatial-resolution TOF MRA at 3.0-T systems offers improved capacity for diagnosis to investigate cerebrovascular disease.[17,18] In our study, we aimed to compare the results of TOF MRA obtained from 3.0 T MRI and 1.5 T MRI systems. However, due to the insufficient number of patients in our study, we were unable to establish a statistically significant comparison. Therefore, we plan to conduct more comprehensive studies in the future to make this comparison.

We hope that our study will contribute to further research on comparisons between non-contrast MRA and DSA, which are used as imaging modalities to determine the treatment and prognosis of atherosclerotic carotid artery diseases.

There are limitations when assessing vascular structures in TOF MRA. Initially, it is important to note that patient movement, particularly during activities such as swallowing and pulsation, can have a detrimental effect on the quality of MRI images. Another issue arises in situations that disrupt the laminar flow of blood. After a severe obstruction in the blood vessel, the flow of blood becomes turbulent instead of laminar, resulting in a "signal void." Due to the possibility of a signal void appearing in both cases of true complete occlusion and slow blood flow distal to severe stenosis, TOF MRA is not a dependable method for distinguishing between these 2 conditions. A further limitation arises from the signal void caused by the 'in-plane' flow that takes place in tortuous blood vessels that are not perpendicular to the imaging plane. In this situation, the extent of stenosis can be overestimated. Our study did not include any patients with tortuous carotid vascular structures. Obtaining the most precise outcome can potentially be achieved by conducting measurements in various planes. A comparable issue can arise during CDUS examinations when assessing tortuous vessels. Tortuous vessels without stenosis exhibit a notable rise in peak systolic velocities.[16,19] Although there are several limitations, the ability to combine TOF MRA with CDUS is a significant advantage, particularly for patients with renal failure or an allergy to contrast material.

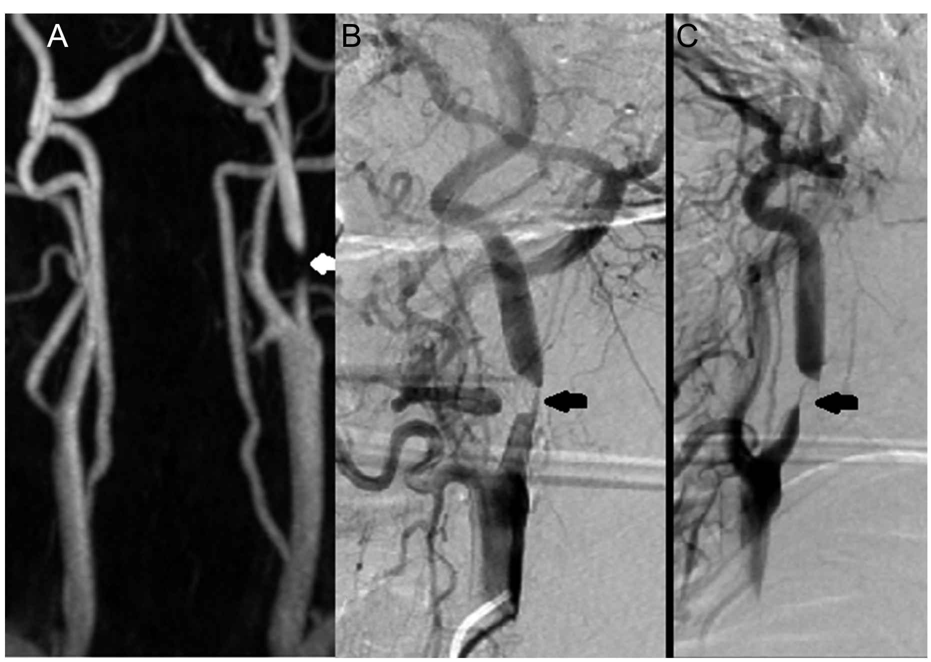

Figure 3. A 70-year-old male patient. He was admitted to our hospital with the complaint of dizziness. While investigating the etiology of vertigo, carotid stenosis was detected in CDUS. In laboratory tests, the creatinine value was found to be 1.2. The patient underwent neck TOF MRA, and carotid DSA procedures in our unit. (A–B) TOF MRA sagittal-oblique MIP images show 50%-69% stenosis (white arrows) in the right ICA proximal part and less than 50% stenosis (white stars) in the left ICA proximal. (C) On DSA examination, a critical stenosis of over 70% is observed in the right proximal ICA (black arrow). (D) In DSA examination, less than 50% stenosis is detected in the left proximal ICA (black star).

Figure 4. A 70-year-old male patient. He was examined in our hospital for right hemiparesis. He has a history of hypertension and diabetes, and a creatinine value of 1.3 in laboratory tests. The patient underwent neck TOF MRA, and carotid DSA procedures in our unit. (A) TOF MRA coronal-oblique MIP images show near-total critical stenosis in the left ICA proximal part (white arrow). (B–C) In DSA examination, near-total critical stenosis is observed in the proximal left ICA on anterior-posterior and lateral views (black arrows).

The biggest reason for these discrepancies is the low number of patients and the low rate of patients with significant stenosis, which are the most important limitations of our retrospective study. This reduces statistical significance and causes "selection" BIAS. Nevertheless, despite the limited sample size, we are still eager to present the significant findings from this study as a preliminary report to the literature. In addition, we could not determine the efficacy of non-contrast MRA in imaging these arteries, as there were not enough patients with critical stenosis in CCA and ECA. Another limitation is that we did not compare the non-contrast MRA findings with 3D rotational DSA images.

CONCLUSION

Non-contrast MRA, which does not contain ionizing radiation and does not require nephrotoxic agents in patients with impaired renal function, can be used as an additional imaging method in cases where CDUS is insufficient in imaging the carotid arteries. Sometimes, it can be used safely in combination with CDUS to increase the accuracy of diagnosis with high sensitivity and specificity.

Ethics Committee Approval: Ethical committee approval was received from Ankara University Faculty of Medicine Clinical Research Ethics Committee (Date: 2014; Decision No: 06-355-18).

Informed Consent: Written informed consent was obtained from the patients who agreed to take part in the study.

Peer-review: Externally peer-reviewed.

Author Contributions: Concept – K.B.M.; Design – A.O.G.; Supervision – K.B.M., U.S.; Resources – K.B.M., A.O.G.; Materials – K.B.M., A.O.G.; Data Collection and/or Processing – K.B.M.; Analysis and/or Interpretation – K.B.M., U.S.; Literature Search – K.B.M., A.O.G.; Writing Manuscript – K.B.M., A.O.G.; Critical Review – K.B.M., U.S.

Declaration of Interests: The authors have no conflict of interest to declare.

Funding: The authors declared that this study has received no financial support.

REFERENCES

1. Paraskevas KI, Mikhailidis DP, Antignani PL, et al. Comparison of recent practice guidelines for the management of patients with asymptomatic carotid stenosis. *Angiology*. 2022;73(10):903-910. [CrossRef]
2. Atman D, Üstüner E, Uzun E, et al. Klinik olarak anlamlı Karotis Arter Stenozlarının Değerlendirilmesinde renkli Doppler Görüntüleme, manyetik rezonans anjiyografi ve dijital Subtraksiyon anjiyografi Yöntemlerinin Karşılaştırılması. *Ank Univ Tıp Fak Mecmuası*. 2014;67(1):5-16. [CrossRef]
3. Heck D, Jost A. Carotid stenosis, stroke, and carotid artery revascularization. *Prog Cardiovasc Dis*. 2021;65:49-54. [CrossRef]
4. Platzek I, Sieron D, Wiggermann P, Laniado M. Carotid artery stenosis: comparison of 3D time-of-flight MR angiography and contrast-enhanced MR angiography at 3T. *Rad Res Pract*. 2014;2014:508715. [CrossRef]
5. Barlinn K, Alexandrov AV. Vascular imaging in stroke: comparative analysis. *Neurotherapeutics*. 2011;8(3):340-348. [CrossRef]
6. Gupta A, Baradaran H, Kamel H, et al. Intraplaque high-intensity signal on 3D time-of-flight MR angiography is strongly associated with symptomatic carotid artery stenosis. *AJNR Am J Neuroradiol*. 2014;35(3):557-561. [CrossRef]
7. Coşkun FY, Yüce M, Özer HO. İnme nedeni olarak Aterosklerotik Karotis Arter hastalığı: risk Faktörlerinin Kontrolünde Medikal yaklaşım. *Turk Klin J Radiol-Spec Top*. 2014;7(3):6-11.
8. Temizöz O, Nayman A, Koç O, Hastalığı AKA. Tanıda dijital çıkartma Anjiyografisi. *Turk Klin J Radiol-Spec Top*. 2014;7(3):45-49.
9. Romero JR, Beiser A, Seshadri S, et al. Carotid artery atherosclerosis, MRI indices of brain ischemia, aging, and cognitive impairment: the Framingham study. *Stroke*. 2009;40(5):1590-1596. [CrossRef]
10. Hathout GM, Fink JR, El-Saden SM, Grant EG. Sonographic NASCET index: a new doppler parameter for assessment of internal carotid artery stenosis. *AJNR Am J Neuroradiol*. 2005;26(1):68-75.
11. Adla T, Adlova R. Multimodality imaging of carotid stenosis. *Int J Angiol*. 2015;24(3):179-184. [CrossRef]
12. Dikici AS, Bakan S, Kantarcı F, Hastalığı AKA. Tanıda Doppler Ultrasonografi. *Turk Klin J Radiol-Spec Top*. 2014;7(3):28-32.

13. Chappell FM, Wardlaw JM, Young GR, et al. Carotid artery stenosis: accuracy of noninvasive tests—individual patient data meta-analysis. *Radiology*. 2009;251(2):493-502. [CrossRef]
14. Wardlaw JM, Chappell FM, Best JJK, Wartolowska K, Berry E, National Health Service Research and Development Health Technology Assessment Carotid Stenosis Imaging Group. Non-invasive imaging compared with intra-arterial angiography in the diagnosis of symptomatic carotid stenosis: a meta-analysis. *Lancet*. 2006;367(9521):1503-1512. [CrossRef]
15. Nederkoorn PJ, van der Graaf Y, Eikelboom BC, van der Lugt A, Bartels LW, Mali WPTM. Time-of-flight MR angiography of carotid artery stenosis: does a flow void represent severe stenosis? *AJNR Am J Neuroradiol*. 2002;23(10):1779-1784.
16. Jaff MR, Goldmakher GV, Lev MH, Romero JM. Imaging of the carotid arteries: the role of duplex ultrasonography, magnetic resonance arteriography, and computerized tomographic arteriography. *Vasc Med*. 2008;13(4):281-292. [CrossRef]
17. Graves MJ. 3 T: the good, the bad and the ugly. *Br J Radiol*. 2022;95(1130):20210708. [CrossRef]
18. Willinek WA, Born M, Simon B, et al. Time-of-flight MR angiography: comparison of 3.0-T imaging and 1.5-T imaging--initial experience. *Radiology*. 2003;229(3):913-920. [CrossRef]
19. Capel KW, Roberts G, Kuner AD, et al. Beyond TOF MRA: review of flow imaging techniques. *Neurographics*. 2023;13(4):294-314. [CrossRef]

Current Research in MRI

Case Report

Intradural Venous Sinus Cyst Mimicking Sinus Vein Thrombosis on Magnetic Resonance Venography

Önder Durmaz[1], Kemal Buğra Memiş[1], Erdal Karavaş[2], Barış İrgül[1]

[1]Department of Radiology, Erzincan Binali Yıldırım University, Faculty of Medicine, Erzincan, Türkiye
[2]Department of Radiology, Bandırma Training and Research Hospital, Balıkesir, Türkiye

Cite this article as: Durmaz Ö, Memiş KB, Karavaş E, İrgül B. Intradural venous sinus cyst mimicking sinus vein thrombosis on magnetic resonance venography. *Current Research in MRI*, 2024;3(2):57-59.

Corresponding author: Önder Durmaz, e-mail: drmzonder2577@gmail.com

Received: July 19, 2023 **Accepted:** September 5, 2023 **Publication Date:** October 6, 2023

DOI:10.5152/CurrResMRI.2023.23074

Abstract

Cerebral venous thrombosis is the obstruction of cranial venous pathways, including thrombosis in the cortical, dural, and deep cerebral veins. It constitutes 0.5%-1% of all strokes and is usually seen in young people. It is slightly more common in young women due to pregnancy, puerperium, and oral contraceptive use. Patients usually present with headaches or focal neurological deficits. Intradural venous sinus cysts are congenital and very rare pathologies. They are usually asymptomatic and detected incidentally. However, large cysts may be symptomatic when they disrupt the venous flow. Common symptoms are headaches and syncope. In this case, we present our 41-year-old female patient with complaints of headache, syncope, dizziness, ringing in the ears, and sleep disturbances that have been going on for 1 month. The patient's complete blood count revealed a normal hematocrit, hemoglobin, and red blood cell count. After clinical and laboratory exclusion of other differential diagnoses in the case, a magnetic resonance imaging (MRI) venography examination was requested with the preliminary diagnosis of dural sinus vein thrombosis. In the magnetic resonance venography examination performed in our case, an unenhanced 7 mm-diameter area was observed in the contrast-enhanced series. The diagnosis was primarily considered as cerebral venous sinus thrombosis. Our patient's complaints of severe headache, dizziness, and syncope were also consistent with our initial diagnosis. However, our patient did not benefit from the anticoagulant treatment given. For this reason, we turned to alternative diagnoses and performed a contrast-enhanced MRI. Our diagnosis changed to intradural venous sinus cyst after constrast-enhanced MRI examination.

Keywords: Arachnoid, cysts, dural sinuses, MRI

INTRODUCTION

Intradural venous sinus cysts are congenital and very rare pathologies.[1] They are usually asymptomatic and detected incidentally. However, large cysts may be symptomatic when they disrupt the venous flow. Common symptoms are headache and syncope.[2] Similar to other cystic lesions in the body, these lesions measure 0-30 Hounsfield Unit (HU) on brain computed tomography (CT) and appear isodense with cerebrospinal fluid. They are observed as intraluminal filling defects on contrast-enhanced examinations. Intradural venous sinus cysts appear isointense with cerebrospinal fluid in all sequences on MRI, that is, hypointense on T1-weighted and Fluid Attenuated Inversion Recovery (FLAIR) images and hyperintense on T2-weighted images.[2] Differential diagnoses include adipose tissue, arachnoid granulations, aeroceles, and cerebral venous sinus thrombosis.[3,4] Fat tissue is easily distinguished on CT and magnetic resonance (MR) images. Arachnoid granulations can be visualized inside the sinuses. These lesions appear as polypoidal structures in the sinus walls. Although aeroceles can be mistaken for cysts in appearance, a close examination reveals CT intensities of less than 50 HU that appear as signal gaps on all MR sequences.[3]

CASE PRESENTATION

A 41-year-old female patient complained of severe headache, dizziness, and ringing in the ears for 1 month. The patient's complete blood count revealed a normal hematocrit, hemoglobin, and RBC count. After clinical and laboratory exclusion of other differential diagnoses in the case, an MRI venography examination was requested with the preliminary diagnosis of dural sinus vein thrombosis. On MR venography, a lesion thought to be a thrombus was seen in the left transverse sinuses (Figure 1). Thereupon, the patient was hospitalized, and anticoagulant was started. Our patient used anticoagulants; however, she applied to us again with the same complaints. In the tests performed, no problems were found in terms of anticoagulants and thrombophilia. The patient underwent a contrast-enhanced MRI the next day. And an unenhanced 7 mm-diameter area was observed in the contrast-enhanced series in the left transverse sinus (Figure 2). It was later found out that it was a cyst located in the left transverse sinus. Written informed consent was obtained from patient who participated in this study.

DISCUSSION

Intradural venous sinus cysts are congenital and very rare pathologies.[1] They are usually asymptomatic and detected incidentally. However, large cysts may be symptomatic when they disrupt the venous flow. Common symptoms are headache and syncope.[2] Similar to other cystic lesions

Figure 1. In the magnetic resonance venography image, a hypointense lesion (red circle) is seen in the left transverse sinus.

in the body, these lesions measure 0-30 HU on brain CT and appear isodense with cerebrospinal fluid. They are observed as intraluminal filling defects on contrast-enhanced examinations. Intradural venous sinus cysts appear isointense with cerebrospinal fluid in all sequences on MRI, that is, hypointense on T1-weighted and FLAIR images, and hyperintense on T2-weighted images (Table 1).[2]

Differential diagnoses include adipose tissue, arachnoid granulations, aeroceles, and cerebral venous sinus thrombosis.[3,4] Fat tissue is easily distinguished on CT and MR images. Arachnoid granulations can be visualized inside the sinuses. These lesions appear as polypoidal structures in the sinus walls. Although aeroceles can be mistaken for cysts in appearance, a close examination reveals CT intensities of less than 50 HU that appear as signal gaps on all MR sequences (Table 2).[3]

Cerebral venous sinus thrombosis is diagnosed primarily by suspecting the clinical situation and showing thrombosis radiologically. Cerebral venous sinus thrombosis is seen in the superior sagittal and transverse

Table 1. Summary Table of Intradural Venous Sinus Cysts

Etiology	Clearly unknown
Incidence	Very rare
Gender ratio	Not known
Age predilection	Not known
Risk factors	Not known
Treatment	They may yet require conservative or surgical management in symptomatic patients.
Prognosis	
Findings on imaging	0-30 HU is measured on cranial computed tomography and is isodense with cerebrospinal fluid. Intradural venous sinus cysts appear isointense with cerebrospinal fluid in all sequences on MRI.

MRI, magnetic resonance imaging.

sinus thrombosis most frequently. Severe headache, which is the most important complaint of increased intracranial pressure, is seen in 90% of cases.[5]

Although CT and MR venography are the preferred techniques for imaging cerebral venous sinus thrombosis, currently the most basic diagnostic methods are cranial MRI and MR venography. In the MR venography examination performed in our case, an unenhanced 7 mm-diameter area was observed in the contrast-enhanced series. The diagnosis was primarily considered to be cerebral venous sinus thrombosis. Our patient's complaints of severe headache, dizziness, and syncope were also consistent with our initial diagnosis. However, our patient did not benefit from the anticoagulant treatment given. For this reason, we turned to alternative diagnoses and performed a contrast-enhanced MRI. Our diagnosis changed to intradural venous sinus cyst after contrast-enhanced MRI examination.

Similar symptoms in intradural venous sinus cysts and cerebral venous sinus thrombosis were the main factors that misled us. Even though, MR venography is the best method for the diagnosis of cerebral venous sinus thrombosis, this technique can fail to differentiate thrombosis from dural venous sinus cysts. In these kinds of situations, a contrast-enhanced MRI scan can aid to confirm diagnosis.

In conclusion, dural venous sinus cysts are very rare and can be confused with thrombosis by revealing similar symptoms. Contrast-enhanced MRI scans can be the key for differential diagnosis.

Teaching Point

Intradural venous sinus cysts are congenital and very rare pathologies. They are usually asymptomatic and detected incidentally. However,

Figure 2. In the axial T2WI (A), a hyperintense lesion is seen in the left transverse sinus. The lesion shows no enhancement on pre- (B) and post-contrast (C) T1WIs. T1WI, T1-weighted image; T2WI, T2-weighted image.

Table 2. Differential Diagnosis Table for Intradural Venous Sinus Cysts

	CT	MRI
Intradural venous sinus cysts	0-30 HU is measured on cranial CT and is isodense with CSF.	Intradural venous sinus cysts appear isointense with CSF in all sequences on MRI.
Adipose tissue	Higher HU values—fat density	Signal loss in fat-saturated sequences, hyperintense on both T1WI and T2WI
Arachnoid granulations	These lesions appear as polypoidal structures in the sinus walls.	Signal characteristics are generally those of CSF.
Aeroceles	They appear as CT intensities of less than 50 HU.	They appear as signal gaps in all MR sequences.
Cerebral venous sinus thrombosis	Filling defect is visible in the sinus with contrast CT.	It is isointense on T1 sequences and hypointense on T2 sequences throughout the acute phase. It becomes hyperintense on T1 sequences during the subacute phase.

CSF, cerebrospinal fluid; CT, computed tomography; MRI, magnetic resonance imaging; T1WI, T1-weighted image; T2WI, T2-weighted image.

large cysts may be symptomatic when they disrupt the venous flow. Common symptoms are headaches and syncope. Contrast-enhanced MRI scans can be the key for differential diagnosis.

Informed Consent: Written informed consent was obtained from patient who agreed to take part in the study.

Peer-review: Externally peer-reviewed.

Author Contributions: Concept – Ö.D.; Design – Ö.D., K.B.M.; Supervision – E.K.; Resources – Ö.D., K.B.M.; Materials – Ö.D.; Data Collection and/or Processing – B.İ.; Analysis and/or Interpretation – E.K.; Literature Search – Ö.D., B.İ.; Writing Manuscript – Ö.D., E.K.; Critical Review – E.K., Ö.D.; Other – Ö.D.

Declaration of Interests: The authors have no conflict of interest to declare.

Funding: The authors declared that this study has received no financial support.

REFERENCES

1. Inagaki T, Yamanouchi Y, Nishimura T, Kawamura Y, Kawamoto K. Intracranial dural cyst. *Childs Nerv Syst*. 1998;14(1-2):69-73. [CrossRef]
2. Ojemann JG, Moran CJ, Gokden M, Dacey RG Jr. Sagittalsinusocclusi onbyintraluminal dural cysts. Report of two cases. *J Neurosurg*. 1999;91(5):867-870. [CrossRef]
3. Rastogi R. Intraluminal dural venoussinuscystsimulating as aerocele in computerizedtomographybrain. *Ann Indian Acad Neurol*. 2008;11(2):116-118. [CrossRef]
4. Balo J. The dural venoussinuses. *Anat Rec*. 1950;106(3):319-324. [CrossRef]
5. Rodallec MH, Krainik A, Feydy A, et al. Cerebralvenousthrombosisa ndmultidetector CT angiography: tipsandtricks. *RadioGraphics*. 2006;26(suppl 1):S5-18; discussion S42. [CrossRef]

Current Research in MRI

Case Report

Cytotoxic Lesions of the Corpus Callosum: A Case Series

Leyla Mirzayeva, Nil Tokgöz, Emetullah Cindil

Department of Radiology, Gazi University Faculty of Medicine, Ankara, Türkiye

Cite this article as: Mirzayeva L, Tokgöz N, Cindil E. Cytotoxic lesions of the corpus callosum: A case series. *Current Research in MRI*, 2024;3(2):60-64.

Corresponding author: Leyla Mirzayeva, e-mail: leyla.salimli91@gmail.com

Received: November 11, 2023 **Revision Requested:** December 28, 2023 **Last Revision Received:** January 4, 2024 **Accepted:** January 8, 2024
Publication Date: August 22, 2024

DOI:10.5152/CurrResMRI.2024.23083

Abstract

Various clinical conditions such as encephalitis, spontaneous intracranial hypotension, childbirth, trauma, use of antipsychotic and chemotherapeutic drugs, and subarachnoid hemorrhage may cause high-signal lesions in the splenium of the corpus callosum on diffusion-weighted imaging, which are referred to as cytotoxic lesions of the corpus callosum. In this article, we aimed to present the cytotoxic lesions of the corpus callosum, which were detected incidentally in patients who underwent brain magnetic resonance imaging for different reasons in our center.
Keywords: Corpus callosum, cytotoxic lesion, MRI, neuroimaging

INTRODUCTION

Cytotoxic lesions of the corpus callosum (CLOCCs) are clinical–radiological conditions characterized by a specific magnetic resonance imaging (MRI) pattern. Causes of CLOCCs include various entities such as drug therapy, malignancy, infection, subarachnoid hemorrhage, metabolic disorders, trauma, spontaneous intracranial hypotension, and the early postpartum period.[1-4] Since CLOCCs are secondary lesions associated with various clinical conditions, it is important for radiologists to know their causes in order to guide treatment.

In general, MRI shows a round lesion in the mid-splenium of the corpus callosum that is hyperintense on T2-weighted (T2W)/fluid-attenuated inversion recovery (FLAIR) sequences. Lesions show no enhancement on contrast-enhanced (CE) T1-weighted images (T1WI). The most important imaging finding is the restricted diffusion in diffusion-weighted imaging (DWI). In CLOCCs, the CC can be affected in 3 different patterns: 1) a round/oval lesion in the center of the splenium; 2) a lesion extending from the mid-splenium to either side with commissural fibers; and 3) a lesion extending from the splenium to the body of the CC.[5] We report here 5 cases of CLOCCs with different causes.

CASE PRESENTATION

Case 1

A 50-year-old man with orthostatic headache presented with severe headache and nausea. On physical examination, he was conscious and oriented, and no deficits in muscle strength and dizziness were observed. The patient underwent cranial MRI (Figures 1A-G) and magnetic resonance venography (MRV) (Figure 1H). MRI revealed a subdural hematoma (SDH) in the right hemisphere, subdural effusion in the left hemisphere, thinning of the lateral ventricles, 5 mm displacement of the cerebellar tonsils caudally at the level of the foramen magnum, and narrowing of the mamillopontine space (3 mm) (Figures 1A-E). There was a well-circumscribed, round-shaped non-enhancing lesion in the splenium of the CC (Figures1A-E), which was hyperintense on T2W/FLAIR sequences and was accompanied by marked restricted diffusion (Figures 1F and G). Post-contrast MRI images revealed leptomeningeal enhancement of the brain (Figures 1D and E). In addition, cortical veins, superior and inferior sagittal sinuses, and sinus rectus were prominent on the cranial MRV (Figure 1H). The findings were consistent with the diagnosis of intracranial hypotension. Lumbar epidural blood patch treatment was performed with 25 mL of autologous venous blood at the L4–L5 intervertebral level, and burr-hole evacuation was performed for SDH. After the procedures, the orthostatic headache improved, and the patient was discharged.

Case 2

A 19-year-old female applied to the emergency department of our institution with confusion after falling off a horse. The values of laboratory tests, including a hemogram, renal and liver function tests, and a serum electrolyte analysis, were within normal limits. The patients brain computed tomography revealed linear hemorrhagic densities in the subcortical white matter of both frontal lobes (Figure 2). An oval-shaped T2W/FLAIR hyperintense lesion (Figure 3A) with restricted diffusion on DWI (Figures 3B and C) was observed in the splenium of the CC. Multiple hemorrhagic foci were detected in bilateral periventricular and subcortical white matter on susceptibility-weighted imaging (SWI) images (Figures 3D-F). Findings were consistent with posttraumatic diffuse axonal injury and CLOCCs. The patient received levetiracetam, cefazolin, haloperidol, and mannitol treatment for 4 days. The patient's consciousness improved after the treatment, and she was discharged on the fifth day.

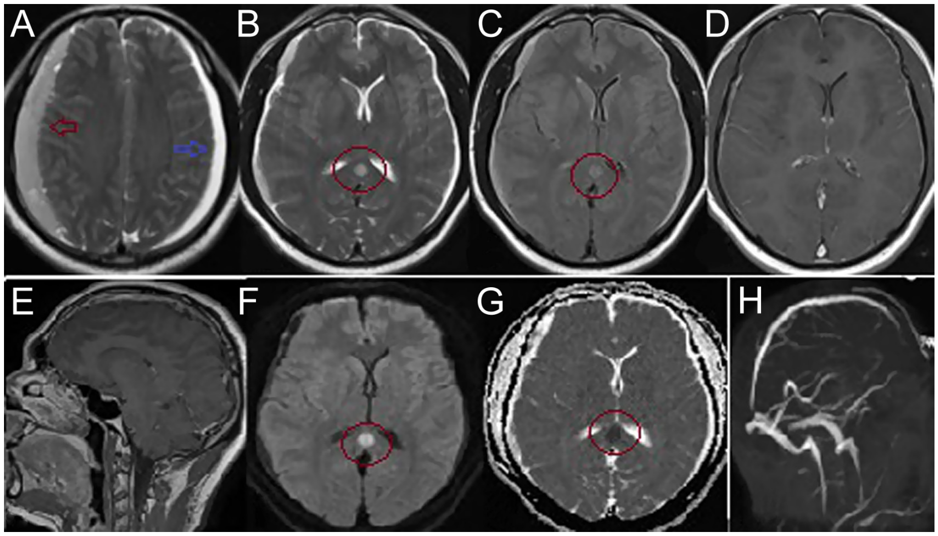

Figure 1. T2-weighted axial image (A) shows a subdural hematoma in the right hemisphere (red arrow) and subdural effusion in the left hemisphere (blue arrow). Axial T2-weighted (B) and fluid-attenuated inversion recovery (C) images demonstrate a round focal hyperintense lesion in the mid-splenium of the corpus callosum (circles). Axial (D) and sagittal (E) contrast-enhanced T1-weighted images show a lack of lesion enhancement but diffuse leptomeningeal enhancement. The lesion reveals restricted diffusion with a hyperintense signal on the diffusion weighted image (F, circle) and hypointensity on the apparent diffusion coefficient map (G, circle). Axial images (B-D) show thinning of the lateral ventricles. There is a caudal displacement in the cerebellar tonsils on the sagittal contrast-enhanced T1-weighted image (E). Enlargement of the cortical veins, superior and inferior sagittal sinuses, and sinus rectus was observed in cranial magnetic resonance venography (H).

Case 3

A 30-year-old female presented with headache and bilateral temporary visual impairment episodes lasting for 1 week on the 20th day of the postpartum period. She had no history of neurological disease or hypertension. No abnormality was observed in neurological and ophthalmological examinations. Complete blood count parameters and blood biochemical tests, including thyroid hormone and cholesterol levels, were normal. Although mean ambulatory blood pressure measurements were normal, spot-high values were detected in the range of 160-170/100-110 mm Hg. Mild proteinuria was detected in the patient's urinalysis. Based on clinical and laboratory findings, it was diagnosed as late-onset preeclampsia. There was an ovoid T2W/FLAIR hyperintense splenial lesion (Figures 4A and B) showing restricted diffusion with markedly low apparent diffusion coefficient (ADC) values on MRI (Figures 4C and D). Clinical symptoms resolved within a week, and a control MRI performed 3 weeks later showed the complete disappearance of the callosal lesion (Figures 4E-H).

MAIN POINTS

- The corpus callosum is a special region of the brain that is sensitive to trauma, drugs, and inflammatory processes due to the large number of excitatory amino acid receptors, cytokine receptors, and drug receptors it contains.
- Diffusion-weighted images and T2-weighted/fluid-attenuated inversion recovery magnetic resonance imaging sequences are crucial for diagnosis as they can identify cytotoxic lesions of the corpus callosum (CLOCCs), which lack a mass effect and do not enhance with contrast medium.
- Knowing the causes of CLOCCs and evaluating the patient with a clinical history will facilitate the radiologist in the differential diagnosis of conditions that have a similar appearance.

Case 4

A 26-year-old male patient who had bipolar disorder was admitted to the emergency department with a psychotic attack. At presentation, blood pressure was 160/90 mm Hg, and his pulse rate was 90 beats/min.He was under treatment with olanzapine and a brain MRI was performed to rule out organic causes. On MRI, there was a round hyperintense lesion on T2W and FLAIR sequences in the mid-splenium of CC (Figures 5A and B). The lesion showed restricted diffusion with a hyperintense signal on the DWI (C) and a hypointense signal on the ADC map (D). The patient's clinical condition was evaluated as olanzapine-induced mania. After sedation with a combination of lorazepam and haloperidol, he was referred to the psychiatric department to re-evaluate the use of olanzapine.

Case 5

A 24-year-old female patient developed blurred vision and diplopia while being followed up in the infectious diseases department with encephalitis. In cerebrospinal fluid analysis, no abnormal finding was detected except the low protein value (8 mg/dl). Then the patient underwent a brain MRI. On the MRI, although visual pathways, pituitary gland, and primary motor cortex were in normal appearance,

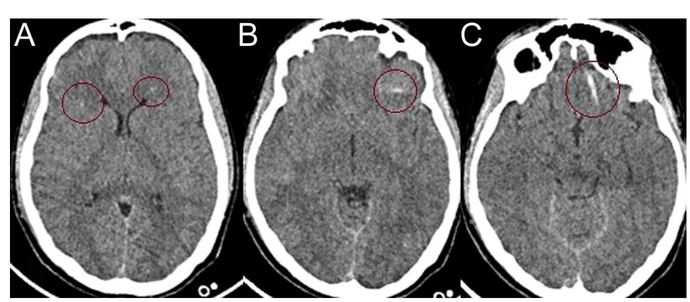

Figure 2. Subcortical linear hemorrhagic densities are shown in both frontal lobes on axial computed tomography images (A-C, circles).

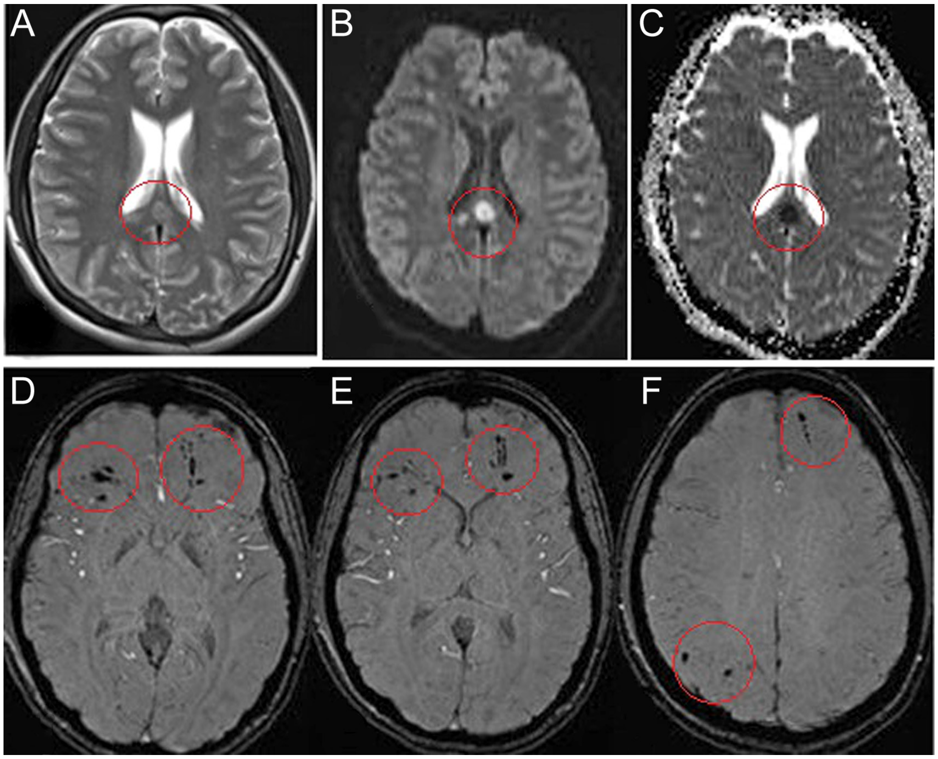

Figure 3. There is a round-shaped hyperintense focal lesion on the T2-weighted image (A, circle) in the mid-splenium of the corpus callosum with restricted diffusion, showing a hyperintense signal on the diffusion-weighted image (B, circle) and a hypointense signal on the apparent diffusion coefficient map (C, circle). SWI images (D-F, circles) show multiple hemorrhagic foci in periventricular and subcortical white matter.

there was a round-shaped lesion in the mid-splenium of the CC, which was hyperintense on T2W/FLAIR sequences (Figures 6A and B) and was accompanied by restricted diffusion on DWI images (Figures 6C and D). The MRI findings were consistent with CLOCCs. The patient received antibiotics (ceftriaxone and vancomycin) and supportive treatment. Her visual complaints improved within 72 hours following the therapy. Written informed consent was obtained from the patients who agreed to take part in the study.

DISCUSSION

CLOCCs take place in the literature with various expressions such as "mild encephalopathy with reversible splenial lesions (MERS),"

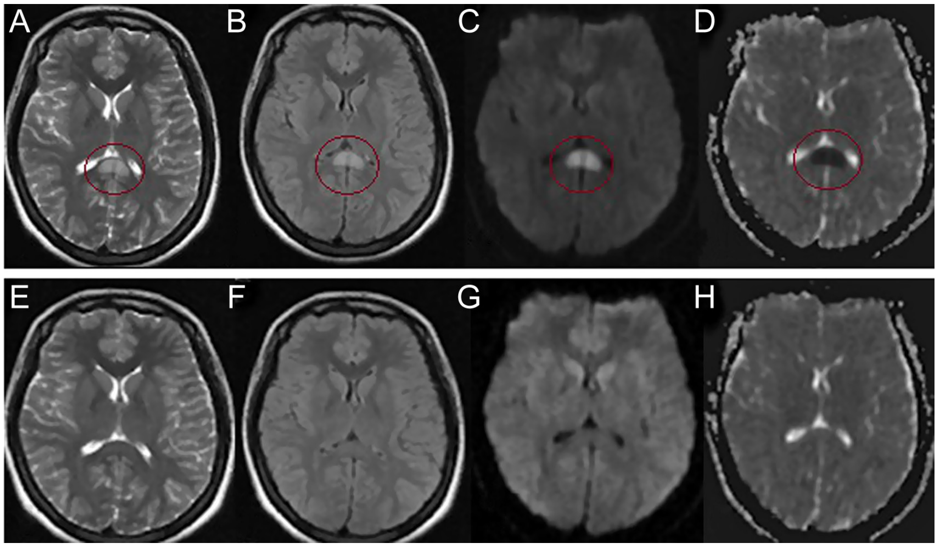

Figure 4. Magnetic resonance image reveals an oval-shaped T2-weighted/fluid-attenuated inversion recovery hyperintense focal lesion in the mid-splenium of the corpus callosum (A-B, circle) with restricted diffusion showing a hyperintense signal on diffusion-weighted imaging (C, circle) and a hypointense signal on the apparent diffusion coefficient map (D, circle). Third-week follow-up magnetic resonance imaging with T2-weighted imaging (E), fluid-attenuated inversion recovery (F), diffusion-weighted imaging (G), and apparent diffusion coefficient mapping (H) reveal the complete disappearance of the callosal lesion.

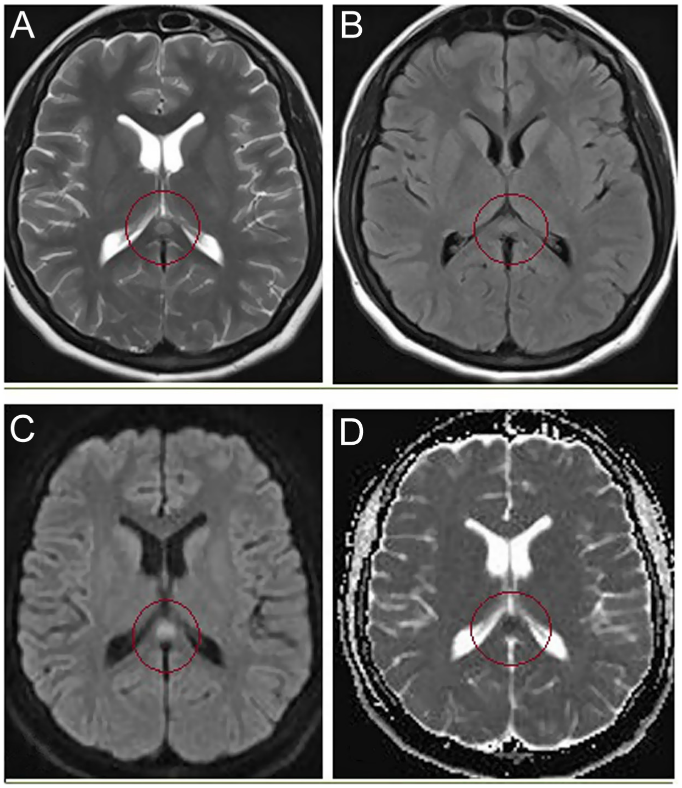

Figure 5. Magnetic resonance imaging shows a round lesion in the mid-splenium of the corpus callosum, which is hyperintense on T2-weighted (A, circle) and fluid-attenuated inversion recovery (B, circle) images. The lesion reveals restricted diffusion with a hyperintense signal on diffusion-weighted imaging (C, circle) and a hypointense signal on the apparent diffusion coefficient map (D, circle).

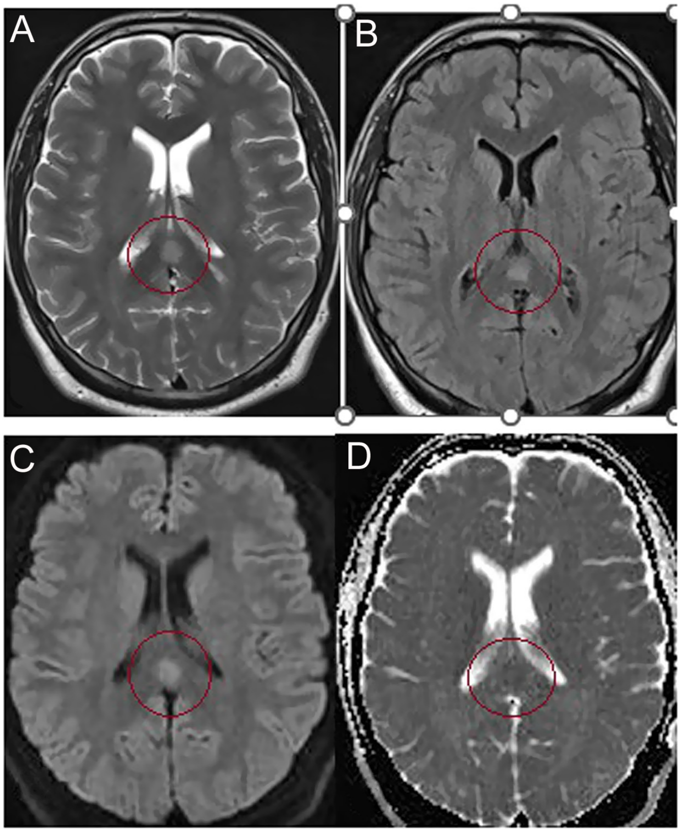

Figure 6. T2-weighted (A, circle) and fluid-attenuated inversion recovery (B, circle) axial images reveal a hyperintense round lesion in the splenium of the corpus callosum. The lesion shows restricted diffusion with a high signal on diffusion-weighted imaging (C, circle) and a low signal on the apparent diffusion coefficient (D, circle).

"reversible splenial lesion syndrome," and "clinically silent lesions in the splenium of the corpus callosum."[6-9] However, splenial lesions of the CC may not always be accompanied by encephalopathy and are not always completely reversible. It has been reported in the literature that restricted diffusion in the splenium of the CC can lead to gliosis.[11]

Recent studies have shown that these callosal lesions with significant diffusion restriction are caused by cytotoxic edema.[5] Trauma, infection, and inflammation activate macrophages and release inflammatory cytokines such as IL-1 and IL-6, initiating the cascade that leads to cytokinopathy. Interleukin 1-stimulated astrocytes secrete glutamate and increase its extracellular level by blocking its reuptake. With a stimulating effect on *N*-methyl-D-aspartate receptors, α-amino-3-hydroxy-5-methyl-4-isoxazole propionic acid receptors, sodium–potassium pumps, and aquaporins, glutamate causes the trapping of water molecules inside neurons.[5-7] This condition results in intracellular edema and restricted diffusion on ADC maps. The splenium of the CC is vulnerable to cytokinopathy. Compared with other brain areas, the neurons and oligodendrocytes of the corpus callosum have a higher density of cytokine receptors, glutamate and other excitatory amino acid receptors, and drug receptors.[10] Therefore, when cytokinopathy occurs, there is a tendency for cytotoxic edema to present in the splenium of the CC. In this case series, we reported 5 patients with different histories and conditions, each showing a similar lesion in the splenium of the CC.

The use of antiepileptic and antipsychotic drugs has an important role in the development of CLOCCs.[12] One of them is olanzapine, an atypical antipsychotic used by 1 patient in our series who had bipolar disorder. Kaino K. et al previously reported the pathophysiological mechanism of the splenial lesion resulting from the use of olanzapine for bipolar disease.[13] Olanzapine toxicity leads to intramyelinic edema and increased inflammatory cytokines; thus, hyperosmolar hyperglycemic state and neuroleptic malignant syndrome occur, which cause CLOCCs.

Although rare, CC lesions associated with postpartum late-onset preeclampsia have been reported in the literature.[14,15] As a result of hormonal and metabolic changes throughout pregnancy, vascular tone regulation may be affected during parturition and may lead to the formation of CLOCCs.[16] However, the pathogenesis of this condition is still not well understood.

It is crucial to differentiate CLOCCs from demyelination, infarction, posterior reversible encephalopathy syndrome (PRES), trauma, and tumors to avoid the wrong and unnecessary treatment. Each of these conditions tends to be asymmetric compared to CLOCCs, which are usually symmetric. Patients with multiple sclerosis typically have ovoid lesions perpendicular to the ventricular axis located in the pericallosal white matter. In PRES, the posterior circulation is typically affected, and MRI usually shows vasogenic edema in the bilateral parietooccipital regions without restricted diffusion or pathological enhancement. Multifocal vasospasm segments in the anterior, middle, and posterior cerebral arteries on MRA images may be helpful in differentiating PRES syndrome from CLOCCs.[17] Entities including lymphoma and glioma may affect the same regions but show a more aggressive appearance with pathological contrast enhancement and vasogenic or infiltrative edema in the surrounding tissue. In addition, necrotic and hemorrhagic components are quite common in glioblastomas.

To summarize, the splenium of the CC is susceptible to trauma, infection, intracranial hypotension, and drug use due to the large number of receptors it contains. If there is a well-circumscribed, round, or oval-shaped isolated lesion in the splenium of the CC that restricts diffusion but does not enhance and is not accompanied by edema in the surrounding parenchyma, CLOCCs should be considered first in the differential diagnosis. In conclusion, knowing the clinical conditions that may lead to CLOCCs and being familiar with typical MRI findings are very important in making the differential diagnosis from other diseases and giving appropriate treatment.

Informed Consent: Written informed consent was obtained from the patiens who agreed to take part in the study.

Peer-review: Externally peer-reviewed.

Author Contributions: Concept – L.M.; Design – X.L.M.; Supervision – N.T.; Materials – N.T., E.C.; Data Collection and/or Processing – L.M., E.C.; Literature Search – L.M.; Writing Manuscript – L.M., N.T.; Critical Review – N.T.

Declaration of Interests: The authors have no conflict of interest to declare.

Funding: The authors declared that this study has received no financial support.

REFERENCES

1. Grosset L, Hosseini H, Bapst B, et al. Mild encephalopathy with reversible splenial lesion: description of nine cases and review of the literature. *Seizure*. 2021;88:83-86. [CrossRef]
2. Dong K, Zhang Q, Ding J, et al. Mild encephalopathy with a reversible splenial lesion mimicking transient ischemic attack: A case report. *Med (Baltim)*. 2016;95(44):e5258. [CrossRef]
3. Ohashi E, Hayakawa I, Abe Y, Tsutsumi Y, Kubota M. Transient Probst bundle diffusion restriction: an acute encephalopathy equivalent to clinically mild encephalopathy with a reversible splenial lesion. *Intern Med*. 2021;60(16):2667-2670. [CrossRef]
4. Moreau A, Ego A, Vandergheynst F, et al. Cytotoxic lesions of the corpus callosum (CLOCCs) associated with SARS-CoV-2 infection. *J Neurol*. 2021 May;268(5):1592-1594. [CrossRef]
5. Starkey J, Kobayashi N, Numaguchi Y, Moritani T. Cytotoxic lesions of the corpus callosum that show restricted diffusion: mechanisms, causes, and manifestations. *RadioGraphics*. 2017;37(2):562-576. [CrossRef]
6. Kim TY, Park DW, Park CK, Lee YJ, Lee SR. Reversible splenial lesion in the corpus callosum on MRI after ingestion of a herbicide containing glufosinate ammonium: a case report. *J Korean Soc Radiol*. 2014;70(6):399-402. [CrossRef]
7. Fujiki Y, Nakajima H, Ito T, Kitaoka H, Takahashi Y. A case of clinically mild encephalitis/encephalopathy with a reversible splenial lesion associated with anti-glutamate receptor antibody [in Japanese]. *Rinsho Shinkeigaku*. 2011;51(7):510-513. [CrossRef]
8. Bulakbasi N, Kocaoglu M, Tayfun C, Ucoz T. Transient splenial lesion of the corpus callosum in clinically mild influenza-associated encephalit is/encephalopathy. *AJNR Am J Neuroradiol*. 2006;27(9):1983-1986.
9. Takanashi J, Shiihara T, Hasegawa T, et al. Clinically mild encephalitis with a reversible splenial lesion (MERS) after mumps vaccination. *J Neurol Sci*. 2015;349(1-2):226-228. [CrossRef]
10. Goursaud S, Kozlova EN, Maloteaux JM, Hermans E. Cultured astrocytes derived from corpus callosum or cortical grey matter show distinct glutamate handling properties. *J Neurochem*. 2009;108(6):1442-1452. [CrossRef]
11. Hashimoto Y, Takanashi J, Kaiho K, et al. A splenial lesion with transiently reduced diffusion in clinically mild encephalitis is not always reversible: A case report. *Brain Dev*. 2009;31(9):710-712. [CrossRef]
12. Polster T, Hoppe M, Ebner A. Transient lesion in the splenium of the corpus callosum: three further cases in epileptic patients and a pathophysiological hypothesis. *J Neurol Neurosurg Psychiatry*. 2001;70(4):459-463. [CrossRef]
13. Kaino K, Kumagai R, Furukawa S, et al. Reversible splenial lesion syndrome with a hyperosmolar hyperglycemic state and neuroleptic malignant syndrome caused by olanzapine. *J Diabetes Investig*. 2017;8(3):392-394. [CrossRef]
14. Takahashi Y, Hashimoto N, Tokoroyama H, et al. Reversible splenial lesion in postpartum cerebral angiopathy: a case report. *J Neuroimaging*. 2014;24(3):292-294. [CrossRef]
15. Hiraga A, Koide K, Aotsuka Y, Kuwabara S. Reversible cerebral vasoconstriction syndrome with transient splenial lesions after delivery. *Intern Med*. 2016;55(22):3357-3359. [CrossRef]
16. Saif H, Valavanis A, Johnson D. A rare case of reversible splenial lesion in third trimester. *Radiol Case Rep*. 2021;16(10):3081-3083. [CrossRef]
17. Parasher A, Jhamb R. Posterior reversible encephalopathy syndrome (PRES): Presentation, diagnosis and treatment [presentation]. *Postgrad Med J*. 2020;96(1140):623-628. [CrossRef]

Current Research in MRI

Vertebral Artery Fenestration: A Rare Vascular Variation Case Report

Huseyin Aydemir[1], Hakki Yesilyurt[2], Taner Koseturk[3]

[1]Department of Radiology, Tokat Erbaa State Hospital, Tokat, Türkiye
[2]Department of Anatomy, Yüksek İhtisas University Faculty of Medicine, Ankara, Türkiye
[3]Department of Anatomy, Erzincan Binali Yıldırım University Faculty of Medicine, Erzincan, Türkiye

Cite this article as: Aydemir H, Yesilyurt H, Koseturk T. Vertebral artery fenestration: A rare vascular variation case report. *Current Research in MRI*, 2024;3(2):65-67.

Corresponding author: Huseyin Aydemir, e-mail: aydemir334@hotmail.com

Received: January 11, 2024 **Revision Requested:** January 29, 2024 **Last Revision Received:** January 29, 2024 **Accepted:** January 31, 2024
Publication Date: March 21, 2024

DOI:10.5152/CurrResMRI.2024.24090

Abstract

Vertebral artery fenestration (VAF) is a rare congenital vascular anomaly that is discovered by incidental during imaging studies of patients who do not exhibit associated symptoms or who have intracerebral hemorrhage as a result of concurrent artery aneurysm or arteriovenous malformations. During catheter angiography, VAF may be mistakenly identified as dissection, hypoplasia, or stenosis. This case report describes a left VAF that was incidentally discovered during magnetic resonance angiography (MRA) utilizing the time-of-flight method.

Keywords: Magnetic resonance angiography, Vertebral artery, Fenestration

INTRODUCTION

Vertebral artery fenestration (VAF) is an uncommon congenital vascular anomaly that can occur extracranially or intracranially. It is defined by a localized split of the vertebral artery (VA) into two parallel channels that subsequently reunite back to a single arterial lumen.[1] Based on autopsy and angiographic studies, the incidence of VAF is estimated to be between 0.23% and 1.95%.[2] It is critical to distinguish between the terms "duplication" and "fenestration," which are sometimes, though wrongly, used synonymously. A VA with 2 sources, a varied trajectory, and a variable level of fusion in the neck is referred to as duplication. In contrast, fenestration, sometimes known as "partial non-fusion," refers to a single-origin vein containing 2 parallel sections somewhere along its path.[3]

Computed tomography angiography probably has greater sensitivity for dissection diagnosis than MRA or ultrasound relative to conventional angiography.[4] Although VAF is not a diagnostic problem in and of itself, proper VAF diagnosis is critical for several reasons. On imaging, VAF may resemble vertebral artery dissection (VAD), a diagnosis linked with substantial morbidity and even fatality. Vertebral artery dissection imaging findings include vascular stenosis/occlusion, pseudoaneurysm, intimal flap, and double lumen; however, the presence of a double lumen has also been reported in VAF. Failure to distinguish between VAF and VAD may result in higher morbidity from unnecessary treatment, such as anticoagulation, follow-up imaging, and anxiety in patients with VAF who are incorrectly diagnosed with VAD.[1,5,6]

In this case report, we aimed to present a case of left VAF in a 22-year-old male patient, which was detected incidentally on magnetic resonance angiography (MRA) obtained using the time-of-flight technique.

CASE PRESENTATION

A 22-year-old male patient complaining of right-sided headache that had not responded to nonsteroidal anti-inflammatory drug treatment for 2 weeks was admitted to our hospital. The patient had no comorbidities, no history of trauma, and laboratory findings were normal. In the MRA examination performed using the time-of-flight technique to exclude possible intracranial vascular malformation, the left VA was divided into 2 parts in the V4 segment and was observed to be fenestrated at this level, rejoining just before forming the basilar artery (Figure 1).

Consent for publication: The patient signed the required consent documents.On the form, the signer granted permission for patient images and other clinical data to be published in the journal.The patient was aware that all efforts would be made to keep her identity a secret and that neither her name nor initials would be published.

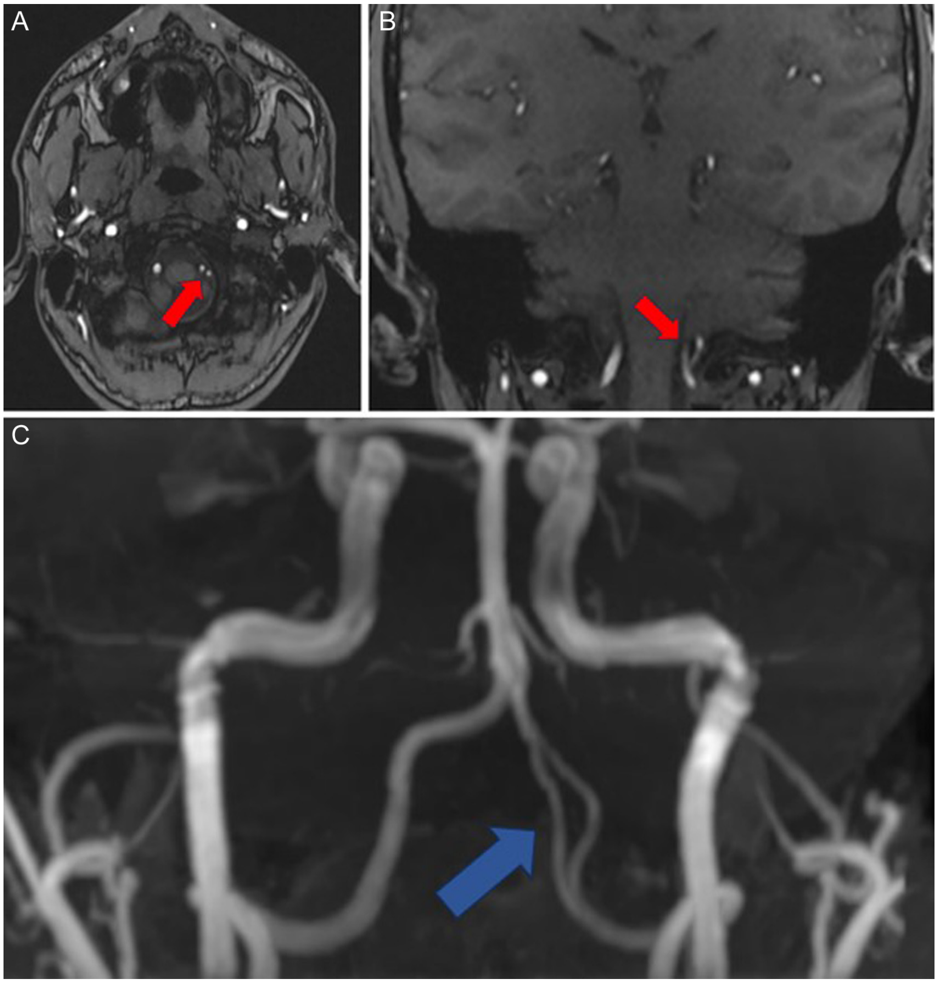

Figure 1. (A, B) In the axial and coronal MRA image, the left VA is divided into 2 parts (red arrows). (C) The maximum intensity projection image shows that the left VA was divided into 2 parts in the V4 segment and was observed to be fenestrated at this level, and rejoining just before forming the basilar artery (blue arrow).

DISCUSSION

The persistence of anastomotic vascular pathways in embryos results in fenestrations. The plexiform anastomoses between the cervical intersegmental arteries that emerge from the aorta give rise to the vertebral arteries during pregnancy.[2,7,8] Vertebral artery fenestration can be seen in the intracranial or extracranial segment of the VA. The extracranial region of the upper cervical level is where it is most prevalent,[9] but the VA's V1 segmental fenestration is incredibly uncommon; in 2013, Gard et al[10] described the first case worldwide.

The clinical significance in this case is the possibility that fenestration of the VA in segment V4 may be confused with VAD. On the other hand, dissections are acquired flaws in the vessel's intima that lead to intramural hematomas that might obstruct or narrow the damaged channel. Dissections may occur spontaneously, after trauma, in people with underlying connective tissue illnesses, or in cases when there are hereditary or environmental risk factors.[1] According to current guidelines, patients diagnosed with VAD should receive antithrombotic therapy, which includes anticoagulant or antiplatelet medications, for 3-6 months. Arterial dissections are usually monitored radiographically over time because they might proceed from focal artery narrowings to frank occlusions or the development of pseudoaneurysms and possible aneurysmal rupture.[11,12] The prognosis for VAD includes the possibility of major disabling deficits and even death in some patients. Incorrect diagnosis of VAD may lead to unnecessary treatment and follow-up imaging risks.[13]

D'Sa et al[1] determined that 9% of patients with intracranial and extracranial VAF had intracranial aneurysms in their study. This is higher than the reported incidence of unruptured intracranial aneurysm in the general population, which is 3.6%-6%.[14] Therefore, it is recommended that identification of VAF on imaging be given greater attention to aneurysms in the same patients.

Herein, the authors present a case of intradural left VAF found incidentally in a man who complained of headache. Fenestrations are an important anatomical variant to appreciate in order to prevent any iatrogenic injuries while caring for patients undergoing endovascular and invasive intracranial interventions. The significance of this case is that it increases our knowledge of uncommon anatomical variations of VA. In this instance, medical professionals can identify the lesions and provide the right treatment to prevent iatrogenic injury. Additionally, this case increases the differential diagnostic spectrum of VAD.

Ethics Committee Approval: N/A.

Informed Consent: Written informed consent was obtained from patients and their relatives who participated in this study.

Peer-review: Externally peer-reviewed.

Author Contributions: Concept – H.A., H.Y.; Design – H.A., T.K.; Supervision – H.Y., T.K.; Materials – H.A.; Data Collection and/or Processing – H.A., H.Y.; Analysis and/or Interpretation – H.Y.; Literature Review – H.A., T.K.; Writing – H.A.; Critical Review – H.A., T.K.

Declaration of Interests: The authors declare that they have no competing interests.

Funding: The authors declare that this study received no financial support.

REFERENCES

1. D'Sa A, Alvin MD, Brody R, Javed S, Faro S, Nadgir RN. Imaging features of vertebral artery fenestration. *Neuroradiology*. 2020;62(5):587-592. [CrossRef]
2. Ozpinar A, Magill ST, Davies JM, McDermott MW. Vertebral artery fenestration. *Cureus*. 2015;7(1):e245. [CrossRef]
3. Ionete C, Omojola MF. MR angiographic demonstration of bilateral duplication of the extracranial vertebral artery: unusual course and review of the literature. *AJNR Am J Neuroradiol*. 2006;27(6):1304-1306.
4. Gottesman RF, Sharma P, Robinson KA, et al. Imaging characteristics of symptomatic vertebral artery dissection: a systematic review. *Neurologist*. 2012;18(5):255-260. [CrossRef]
5. Vertinsky AT, Schwartz NE, Fischbein NJ, Rosenberg J, Albers GW, Zaharchuk G. Comparison of multidetector CT angiography and MR imaging of cervical artery dissection. *AJNR Am J Neuroradiol*. 2008;29(9):1753-1760. [CrossRef]
6. Drapkin AJ. The double lumen: a pathognomonic angiographic sign of arterial dissection? *Neuroradiology*. 2000;42(3):203-205. [CrossRef]
7. Takahashi M, Kawanami H, Watanabe N, Matsuoka S. Fenestration of the extracranial vertebral artery. *Radiology*. 1970;96(2):359-360. [CrossRef]
8. Rieger P, Huber G. Fenestration and duplicate origin of the left vertebral artery in angiography: report of three cases. *Neuroradiology*. 1983;25(1):45-50. [CrossRef]
9. Polguj M, Podgórski M, Jędrzejewski K, Topol M, Majos A. Fenestration and duplication of the vertebral artery: the anatomical and clinical points of view. *Clin Anat*. 2013;26(8):933-943. [CrossRef]
10. Gard AP, Kebriaei MA, Thorell WE. Review of vertebral artery fenestration and novel extracranial fenestration. *Clin Neurol Neurosurg*. 2013;115(7):1107-1109. [CrossRef]
11. Park KW, Park JS, Hwang SC, Im SB, Shin WH, Kim BT. Vertebral artery dissection: natural history, clinical features and therapeutic considerations. *J Korean Neurosurg Soc*. 2008;44(3):109-115. [CrossRef]
12. Chowdhury MM, Sabbagh CN, Jackson D, Coughlin PA, Ghosh J. Antithrombotic treatment for acute extracranial carotid artery dissections: a meta-analysis. *Eur J Vasc Endovasc Surg*. 2015;50(2):148-156. [CrossRef]
13. Arnold M, Bousser MG, Fahrni G, et al. Vertebral artery dissection: presenting findings and predictors of outcome. *Stroke*. 2006;37(10):2499-2503. [CrossRef]
14. Wardlaw JM, White PM. The detection and management of unruptured intracranial aneurysms. *Brain*. 2000;123(2):205-221. [CrossRef]

Current Research in MRI

Case Report

Apical Hypertrophic Cardiomyopathy: A Case Report

Mutlu Buyuklu[1], Duzgun Can Senbil[2], Ayse Sena Celik[2]

[1]Department of Cardiology, Erzincan University Faculty of Medicine, Erzincan, Türkiye
[2]Department of Radiology, Erzincan University Faculty of Medicine, Erzincan, Türkiye

Cite this article as: Buyuklu M, Can Senbil D, Sena Celik A. Apical hypertrophic cardiomyopathy: A case report. *Current Research in MRI*, 2024;3(2):68-70.

Corresponding author: Ayşe Sena Çelik, e-mail: ayse.celik@erzincan.edu.tr

Received: January 16, 2024 **Revision requested:** February 17, 2024 **Last revision received:** February 25, 2024 **Accepted:** March 23, 2024 **Publication Date:** August 21, 2024

DOI:10.5152/CurrResMRI.2024.24091

Abstract

In this case report, a patient with apical hypertrophic cardiomyopathy (AHCM) who presented to the emergency department with chest pain is presented. The symptoms, clinical findings, diagnostic methods, differential diagnosis, and treatment options for apical hypertrophic cardiomyopathy are briefly described. An uncommon type of hypertrophic cardiomyopathy, AHCM typically affects the left ventricle's apex.

Keywords: Cardiomyopathy, hypertrophic cardiomyopathy, magnetic resonance imaging

INTRODUCTION

Apical hypertrophic cardiomyopathy usually affects the apical region of the left ventricle and is morphologically divided into 3 categories: diffuse, focal, and mixed type with interventricular septum hypertrophy. However, this classification is not widely used in clinical practice.

CASE PRESENTATION

A 46-year-old man with no previously known chronic disease presented with chills, tremor in the hands, and chest pain. There was no familial history of sudden cardiac death. Vital findings and physical examination were unremarkable. The electrocardiogram showed deep T negativity in the anterior precordial leads. Laboratory values showed a troponin value of 12 ng/L. On transthoracic echocardiogram, left ventricular ejection fraction was 30%, apex was akinetic, and left ventricular hypertrophy was present. The patient was evaluated with digital subtraction angiography, and no stenosis was detected. The patient was then evaluated with cardiac contrast MRG. Myocardial hypertrophy was observed in the apical septum and left ventricular free wall adjacent to the apex. The apex was relatively thin, and delayed intraventricular contrast evacuation in the apical region was detected in dynamic series. Mid-wall contrast enhancement was present in the apical septum and free wall adjacent to the apex of the left ventricle in late contrast series. The findings were evaluated as AHCMP. The patient was followed up in the cardiology service, and saneloc (50 mg) and panto (40 mg) were started as treatment. An implanted cardiac defibrillator (ICD) was planned for the patient whose risk ratio was above 0.6 in cardiomyopathy risk calculation. Since this case report is retrospective, the need for a consent form was waived.

DISCUSSION

Apical hypertrophic cardiomyopathy is most commonly diagnosed in the middle-age group and is more frequently observed in people of Asian ethnicity.[1] The prevalence of hypertrophic cardiomyopathies in the general population ranges from 0.02% to 0.2%. The incidence of apical hypertrophy is at 1%-2% of all hypertrophied cardiomyopathies compared to 25% in Japan. It is known to affect men more than women.[2] Although autosomal dominant (OD) inheritance has been observed in certain cases of AHCM, the condition is mostly sporadic.[3] In genetically inherited cases, it is known that the alpha cardiac actin gene has a sarcoma mutation called E101K.[4] Patients with AHCM may present with chest pain, dyspnea, palpitations, syncope, atrial fibrillation, myocardial infarction, ventricular rhythm disorders, and heart failure, or may be asymptomatic. The primary diagnostic method for AHCM is a transthoracic echocardiogram. In addition to ECG, multislice spiral CT, left ventriculography, and cardiac magnetic resonance imaging are alternative diagnostic methods.[4] Although transthoracic echocardiogram is the first diagnostic test, the gold standard in diagnosis is cardiac MRI, as stated in various case reports. The cardiac MRI images of apical hypertrophic cardiomyopathy are similar to those of hypertrophied cardiomyopathies. Apical hypertrophic cardiomyopathy holds only the apex. The wall thickness is diagnosed by an intervention septum of 15 mm, a free wall of 10 mm, and mid-wall contrast in late-phase gadolinium images. The traditional appearance of the left ventricle is a configuration resembling a spade or ace-of-spades symbol. A patient with chest pain considered to have apical hypertrophic cardiomyopathy does not need a routine coronary CT scan to rule out other diagnoses. Because of its high spatial resolution, multi-detector computed tomography has recently emerged as a new technique for assessing the morphology and function of the heart. Multi-layered reconstructions allow measurement of heart function as well as myocardial thickness. Cardiac CT can be used to evaluate anatomy in the presence of suboptimal

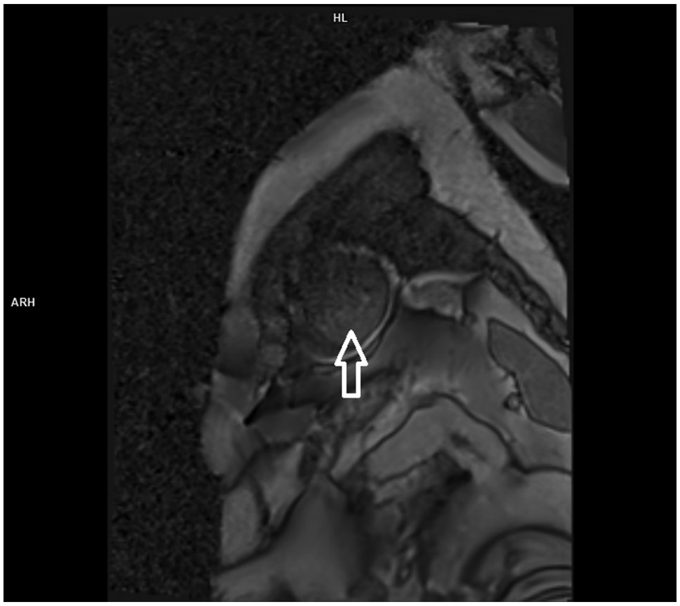

Figure 2. Late-phase gadolinium contrast-enhanced images showed gadolinium uptake in areas of the myocardium with hypertrophy, confirming a diagnosis of focal hypertrophic cardiomyopathy.

echocardiographic images and contraindications of cardium MRI. In this case, the definitive diagnosis was made by cardiac MRI (Figures 1 and 2). As in this case, the most common ECG finding of AHCM is negative T waves in the precordial leads, followed by left ventricular

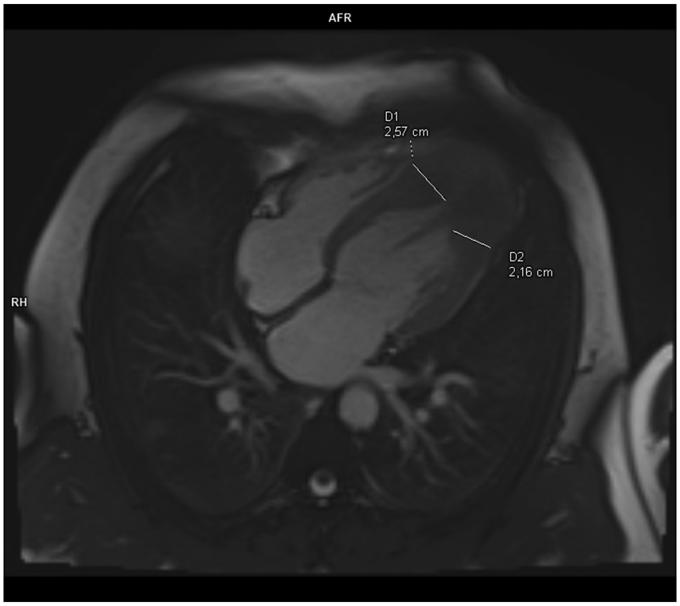

Figure 1. Cine images showed thickening of the apex and interventricular septum surrounding the apex, along with a focal area in the left ventricular free wall. The end-diastolic interventricular septum diameter was 25 mm, and the left ventricular free wall diameter was 21 mm and increased.

hypertrophy (Figure 3). Differential diagnoses may include left ventricular neoplasms, coronary artery disease, endomyocardial fibrosis, and left ventricular apical thrombus. Antiarrhythmic agents such as

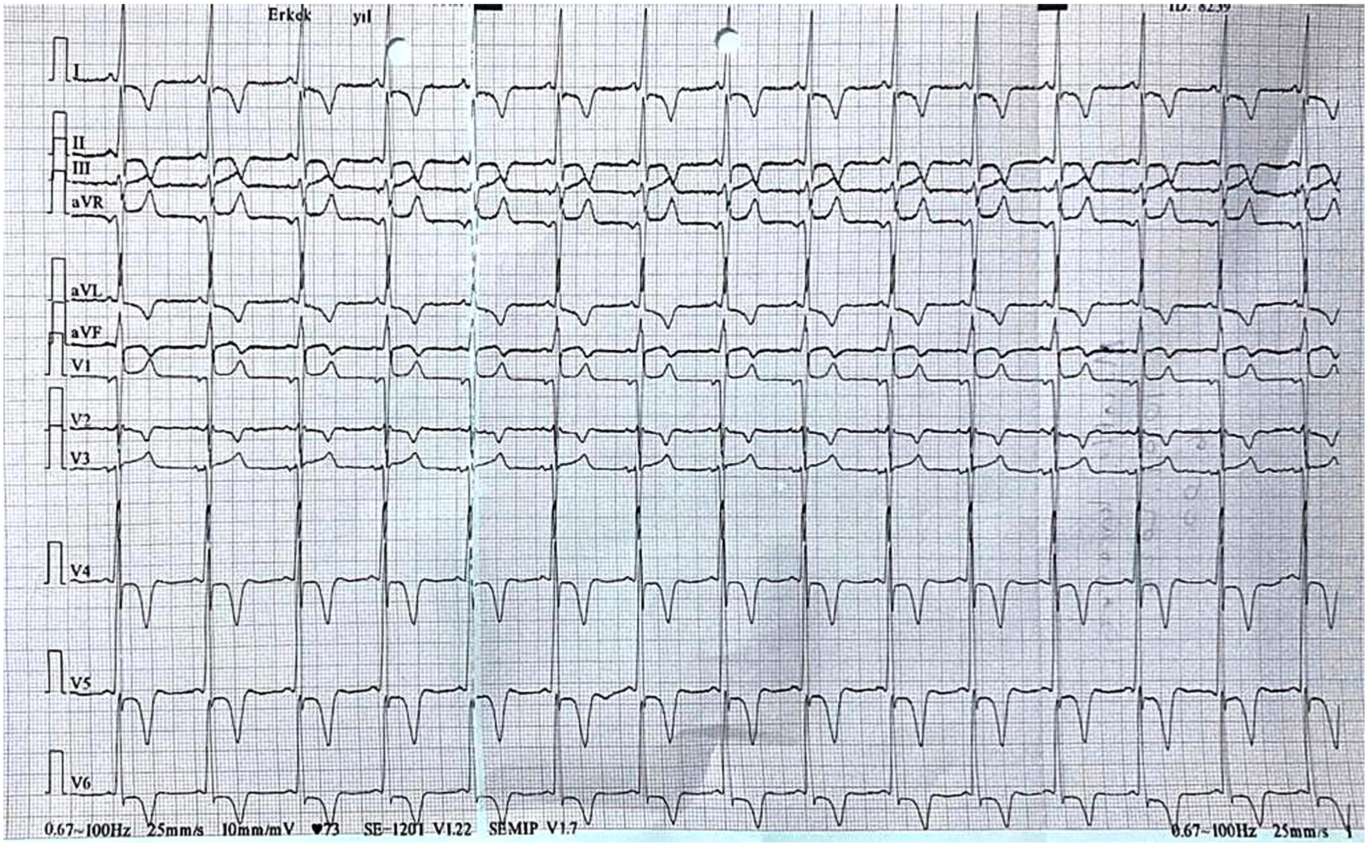

Figure 3. Common T negativity and left ventricular hypertrophy on ECG.

verapamil, beta-blockers, procainamide, and amiodarone are among the medications used to treat AHCM, which usually has a benign course. Implanted cardiac defibrillators, alcohol septal ablation, and apical myomectomy may be treatment options in high-risk patients.

Informed Consent: N/A.

Peer-review: Externally peer-reviewed.

Author Contributions: Concept – M.B.; Design – M.B.; Supervision – M.B.; Materials – D.C.S., A.S.C.; Data Collection and/ Processing – D.C.S., A.C.S.; Analysis and/or Interpretation – D.C.S., A.S.C.; Literature Search – M.B., D.C.S., A.S.C.

Declaration of Interests: The authors have no conflict of interest to declare.

Funding: The authors declared that this study has received no financial support.

REFERENCES

1. Neubauer S, Kolm P, Ho CY, et al. Distinct subgroups in hypertrophic cardiomyopathy in the NHLBI HCM Registry. *J Am Coll Cardiol*. 2019;74(19):2333-2345. [CrossRef]
2. Klarich KW, Attenhofer Jost CH, Binder J, et al. Risk of death in long-term follow-up of patients with apical hypertrophic cardiomyopathy. *Am J Cardiol*. 2013;111(12):1784-1791. [CrossRef]
3. Arad M, Penas-Lado M, Monserrat L, et al. Gene mutations in apical hypertrophic cardiomyopathy. *Circulation*. 2005;112(18):2805-2811. [CrossRef]
4. Yusuf SW, Bathina JD, Banchs J, Mouhayar EN, Daher IN. Apical hypertrophic cardiomyopathy. *World J Cardiol*. 2011 July 26;3(7):256-259. [CrossRef]